Superconducting fluctuations and giant negative magnetoresistance in a gate-voltage tuned two-dimensional electron system with strong spin-orbit impurity scattering

Tsofar Maniv[*] and Vladimir Zhuravlev

Schulich Faculty of Chemistry, Technion-Israel Institute of Technology, Haifa 32000, Israel

We present a quantitative theory of the gate-voltage tuned superconductor-to-insulator transition (SIT) observed experimentally in the 2D electron system created in the (111) interface between crystalline $SrTiO_3$ and $LaAlO_3$. Considering two fundamental opposing effects of Cooper-pair fluctuations—the critical conductivity enhancement, known as paraconductivity, and its suppression associated with the loss of unpaired electrons due to Cooper-pairs formation—we generalize the standard thermal fluctuations theory to include interaction between fluctuations within the self-consistent field approximation and quantum tunneling between mesoscopic superconducting puddles within a phenomenological approach. Relying on the quantitative agreement found between our theory and a large body of experimental sheet-resistance data, we conclude that spin-orbit scatterings, via significant enhancement of the interaction between fluctuations, strongly enhance the sheet resistance peak at high fields and reveal anomalous metallic behavior at low fields, due to mixing of relatively heavy electron bands with a light electron band near a Lifshitz point. The large enhancement of the interaction between fluctuations at high fields, where the sheet resistance is strongly amplified, is shown to result in localization of Cooper-pair fluctuations within mesoscopic puddles.

I. INTRODUCTION

The electron-doped interface between two insulating perovskite oxides—$SrTiO_3$ and $LaAlO_3$—is known to support two-dimensional (2D) high mobility electron systems, providing a great opportunity of tailoring low-dimensional charge states with exotic transport properties [1]. In particular, it has been shown recently [2] that the 2D electron system formed at the $LaAlO_3/SrTiO_3$ (111) interface can be smoothly tuned by gate bias from the superconducting (SC) state deep into an insulating state with pronounced magnetoresistance (MR) peaks developed at low temperatures. Similar electrostatically tuned superconductor-to-insulator transition (SIT) was reported for the $LaAlO_3/SrTiO_3$ (001) interface [3], showing however [4,5] no clear indication of MR peaks similar to those reported for the (111) interface. Earlier studies of the (111) interface have found coexistence of magnetism and 2D superconductivity [6], and a correlation between superconductivity and strong spin-orbit interaction [7]. The linear magnetic field dependence observed at low perpendicular fields and its hysteresis have indicated the importance of flux flow in the detected resistance. These effects persisted deep into the insulating state, revealing the importance of Cooper-pair fluctuations even when superconductivity is completely suppressed. The large smearing of the SC resistive transitions observed under parallel fields may also reflect a strong SC fluctuations effect. The transition temperature T_c and the critical fields, $H_{c\parallel}$, $H_{c\perp}$ for both parallel and perpendicular fields,

respectively, were found [7] to follow nonmonotonic (dome-shaped) gate-voltage dependence of the spin-orbit interaction.

The phenomenon of SIT has been investigated for many years, notably in thin films of materials like bismuth [8], InO [9], MoGe [10], TiN [11], and cuprate superconductors [12]. Many intriguing phenomena have been associated with the observation of SIT. Noteworthy examples are: scaling behavior near a quantum critical point [9,13,14], large MR peaks [11,14,15], and thermally activated insulating behavior [11,14–16]. However, some of these effects have not been observed in all materials that exhibit a SIT, making the interpretation of the various SIT phenomena controversial, with no consensus as to their mechanism and expected behavior.

In this paper we present a scenario of SIT in a 2D electron system, based on the opposing effects generated by fluctuations in the SC order parameter: On one hand, the singular enhancement of conductivity due to fluctuating Cooper pairs in approaching the critical magnetic field (paraconductivity), and on the other hand, the suppression of conductivity associated with the loss of unpaired electrons resulting from Cooper pairs formation. Specializing this scenario to the $LaAlO_3/SrTiO_3$ (111) interface, the strongly enhanced fluctuations effect is due to the remarkable combination of marginal superconductivity driven by spin-orbit scattering versus the pair breaking of Zeeman spin-splitting effect embodied in a 2D electron system. Focusing on the parallel field orientation case enables us to investigate the essence of our model of SIT without interference from the complex vortex kinetics and flux lines pinning processes involved in the perpendicular field case. Furthermore, the striking observations of giant negative MR in both the (111) and the (001) $LaAlO_3/SrTiO_3$ interfaces, driven by spin-orbit coupling under parallel field, at
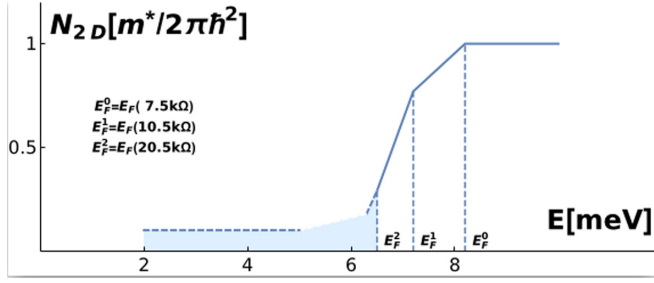
[*]maniv@technion.ac.il

FIG. 1. A three-point histogram of the 2D DOS function extracted in our fitting process from the sheet resistance data for three values of R_N, corresponding to the following values of the Fermi energy: $E_F^0 \equiv E_F(7.5\ k\Omega) = 8.2$ meV, $E_F^1 \equiv E_F(10.5\ k\Omega) = 7.2$ meV, $E_F^2 \equiv E_F(20.5\ k\Omega) = 6.5$ meV (see Appendix B for details). The corresponding values of the interaction parameters are: $\alpha(7.5k\Omega) = 0.09$, $\alpha(10.5k\Omega) = 0.11$, and $\alpha(20.5k\Omega) = 0.30$. The best fitting value found for the band effective mass is $m^* \simeq 1.6m_e$.

temperatures above the SC transition [17,18], are of special interest here: It has been associated [18] with spin-orbit induced band mixing between orbitals of different symmetries near a Lifshitz point in the d-electron interface band structure [19].

We test the validity of the above mentioned SIT scenario by performing calculations based on an effective mixed-bands DOS model and comparing the results with the large body of experimental magnetic sheet resistance (MSR) data presented in Ref. [2]. The calculations were done within an extended version of the Fulde-Maki Aslamazov-Larkin theory of fluctuations in paramagnetically limited superconductors [20–22], in which the linear time-dependent-Ginzburg-Landau (TDGL) equation describing free (Gaussian) fluctuations is modified by taking into account interactions between free fluctuations, self-consistently in the Hartree approximation [23]. Very good quantitative agreement between theory and experiment has been achieved, confirming our SIT scenario. Dynamical quantum tunneling of Cooper-pair fluctuations through GL energy barriers is taken into account, on equal footing with thermal activation, within a phenomenological approach, preserving the high level of agreement with

the experiment in the low temperatures region. Our calculations also reveal how a Lifshitz transition in the d-electron interface band structure [19,24] can drive large enhancements of the MSR peak observed at the end of the SIT path [2] upon gate-voltage variation. This feature is exploited to construct the mixed-band DOS function around the Lifshitz point from the gate-voltage dependent MSR data.

II. THE MODEL AND ITS FORMULATION

We model the perovskite oxides electronic interface state under study here by considering a thin rectangular film of electrons, subject to strong spin-orbit impurity scattering [25,26], under a strong magnetic field H, applied parallel to the conducting plane. We assume, for simplicity of the analysis, that spin-orbit interaction dominates the impurity scatterings. Superconductivity in this system is governed both by the Zeeman spin splitting energy $\mu_B H$ and the spin-orbit scattering rate $1/\tau_{\rm SO} \equiv \hbar/\varepsilon_{\rm SO}$ (see a detailed description in early papers dealing with similar 3D systems [20,27,28]). The underlying spin-orbit induced band mixing, which was evaluated microscopically for the (001) interface by several authors [18,19,29,30], is taken into account here phenomenologically within a minimal model of 2D DOS function $N_{\rm 2D}(E)$ (see Fig. 1 and a more detailed explanation below).

We use a reference of frame in which the conducting interface is in its z-x plane, the film thickness (along the y axis) is d, and $\mathbf{E} = \hat{x}E$, $\mathbf{B} = \hat{z}H$ are the in-plane electric and magnetic fields, respectively. The transport calculations are carried out in the linear response approximation with respect to the electric field and impurity scattering is treated in the dirty limit. To take into account the orbital magnetic field effect one invokes gauge invariance in evaluating the Cooper-pair fluctuations kinetic energy $(1/2)Dq^2$, where D is the electronic diffusion coefficient. Since the film thickness d is much smaller than the Cooper-pair coherence length, this can be done approximately by replacing q^2 with $q_z^2 + \langle (q_x + \frac{2e}{\hbar c}Hy)^2 \rangle = q^2 + (\frac{2e}{\hbar c}H)^2 \langle y^2 \rangle + 2q_x \frac{2e}{\hbar c}H\langle y \rangle = q^2 + 2(edH/\hbar)^2$, where the average is over the narrow film dimension.

Starting with the Nambu field operators:

$$\Psi(\mathbf{r};\tau) \equiv \begin{bmatrix} \psi_\uparrow(\mathbf{r};\tau) \\ \psi_\downarrow(\mathbf{r};\tau) \\ \psi_\uparrow^\dagger(\mathbf{r};\tau) \\ \psi_\downarrow^\dagger(\mathbf{r};\tau) \end{bmatrix}, \quad \Psi^\dagger(\mathbf{r};t) \equiv [\psi_\uparrow^\dagger(\mathbf{r};\tau) \quad \psi_\downarrow^\dagger(\mathbf{r};\tau) \quad \psi_\uparrow(\mathbf{r};\tau) \quad \psi_\downarrow(\mathbf{r};\tau)], \tag{1}$$

the Nambu-Gor'kov time-ordered Green's functions 4×4 matrix is defined by:

$$\mathcal{G}(\mathbf{r}, \mathbf{r}'; \tau, \tau') \equiv -\langle T_\tau \Psi(\mathbf{r};\tau)\Psi^\dagger(\mathbf{r}';\tau') \rangle \equiv \begin{pmatrix} \mathcal{G}_{11}(\mathbf{r}, \mathbf{r}'; \tau, \tau') & \mathcal{G}_{12}(\mathbf{r}, \mathbf{r}'; \tau, \tau') \\ \mathcal{G}_{21}(\mathbf{r}, \mathbf{r}'; \tau, \tau') & \mathcal{G}_{22}(\mathbf{r}, \mathbf{r}'; \tau, \tau') \end{pmatrix}, \tag{2}$$

where T_τ is the time ordered operator and τ, τ' are imaginary (Matsubara) time variables. The 2×2 Green's functions and anomalous Green's functions submatrices relevant to our problem are:

$$\mathcal{G}_{11}(\mathbf{r}, \mathbf{r}'; \tau, \tau') = -\left\langle T_\tau \begin{pmatrix} \psi_\uparrow(\mathbf{r};\tau)\psi_\uparrow^\dagger(\mathbf{r}';\tau') & \psi_\uparrow(\mathbf{r};\tau)\psi_\downarrow^\dagger(\mathbf{r}';\tau') \\ \psi_\downarrow(\mathbf{r};\tau)\psi_\uparrow^\dagger(\mathbf{r}';\tau') & \psi_\downarrow(\mathbf{r};\tau)\psi_\downarrow^\dagger(\mathbf{r}';\tau') \end{pmatrix} \right\rangle,$$

$$\mathcal{G}_{21}(\mathbf{r}, \mathbf{r}'; \tau, \tau') = -\left\langle T_\tau \begin{pmatrix} \psi_\uparrow^\dagger(\mathbf{r};\tau)\psi_\uparrow^\dagger(\mathbf{r}';\tau') & \psi_\uparrow^\dagger(\mathbf{r};\tau)\psi_\downarrow^\dagger(\mathbf{r}';\tau') \\ \psi_\downarrow^\dagger(\mathbf{r};\tau)\psi_\uparrow^\dagger(\mathbf{r}';\tau') & \psi_\downarrow^\dagger(\mathbf{r};\tau)\psi_\downarrow^\dagger(\mathbf{r}';\tau') \end{pmatrix} \right\rangle.$$

In terms of these Green's functions we write the reduced subset of Gor'kov's equations in real space, describing s-wave spin-singlet pairing, as:

$$[(\hbar\partial_\tau - \widehat{\xi})\sigma_0 - \sigma_z\mu_B H]\mathcal{G}_{11}(\mathbf{r}, \mathbf{r}'; \tau, \tau') - \int d^2 r''\mathcal{V}(\mathbf{r}, \mathbf{r}'')\mathcal{G}_{11}(\mathbf{r}'', \mathbf{r}'; \tau, \tau') - i\sigma_y\Delta(\mathbf{r}, \tau)\mathcal{G}_{21}(\mathbf{r}, \mathbf{r}'; \tau, \tau') = \sigma_0\delta(\tau - \tau')\delta(\mathbf{r} - \mathbf{r}')$$
(3)

$$i\sigma_y\Delta^*(\mathbf{r}, \tau)\mathcal{G}_{11}(\mathbf{r}, \mathbf{r}'; \tau, \tau') + [(\hbar\partial_\tau + \widehat{\xi})\sigma_0 + \sigma_z\mu_B H]\mathcal{G}_{21}(\mathbf{r}, \mathbf{r}'; \tau, \tau') + \int d^2 r''\mathcal{V}(\mathbf{r}, \mathbf{r}'')\mathcal{G}_{21}(\mathbf{r}'', \mathbf{r}'; \tau, \tau') = 0$$
(4)

where $\widehat{\xi} = -\hbar^2(\partial_x^2 + \partial_z^2)/2m^* - E_F$, E_F is the Fermi energy, m^* is the electronic band effective mass, $\mu_B = e\hbar/2m_e$ is the Bohr magneton, σ_0, σ_y, σ_z are the 2×2 unity, and the y, z Pauli matrices, respectively, and $\Delta_{\downarrow\uparrow}(\mathbf{r}, \tau) = -\Delta_{\uparrow\downarrow}(\mathbf{r}, \tau) \equiv \Delta(\mathbf{r}, \tau)$—the components of the order-parameter matrix responsible for spin-singlet pairing. In these equations the impurity-scattering matrix is given by [25,26]:

$$\mathcal{V}(\mathbf{r}, \mathbf{r}') = \frac{1}{d}\sum_n \int \frac{d^2 p}{(2\pi)^2} \int \frac{d^2 q}{(2\pi)^2} \exp\left\{i\mathbf{p}\cdot\left[\frac{1}{2}(\mathbf{r} + \mathbf{r}') - \mathbf{R}_n\right] + i\mathbf{q}\cdot(\mathbf{r} - \mathbf{r}')\right\}(iV_{\mathrm{SO}}[\widehat{\mathbf{p}} \times \widehat{\mathbf{q}}]\cdot\sigma),$$
(5)

where $\mathbf{R}_n$ is a position vector of an impurity and $[\widehat{\mathbf{p}} \times \widehat{\mathbf{q}}]\cdot\sigma = \pm|\widehat{\mathbf{p}} \times \widehat{\mathbf{q}}|\sigma_y$, depending on whether $[\widehat{\mathbf{p}} \times \widehat{\mathbf{q}}]$ is oriented parallel $(+)$ or antiparallel $(-)$ to the y axis. The strong spin-orbit interaction of the Ti $3d$ conduction electrons with lattice ions in SrTiO$_3$ [31] motivates our use of Eq. (5) as the spin-orbit impurity scattering matrix of free electrons in the LAO/STO (111) interface.

The temporal Fourier transform, with the fermionic Matsubara frequency, $\omega_n = (2n + 1)\pi k_B T/\hbar$, of the integral equation for the normal state Green's functions matrix $\widetilde{\mathcal{G}}_{11}^{(0)}(\mathbf{r}, \mathbf{r}'; \omega_n)$ in the presence of the spin-orbital impurity scattering, obtained from Eq. (3) with $\Delta(\mathbf{r}, \tau) = 0$, is written as:

$$\widetilde{\mathcal{G}}_{11}^{(0)}(\mathbf{r}, \mathbf{r}'; \omega_n) = \mathcal{G}_{11}^{(0)}(\mathbf{r}, \mathbf{r}'; \omega_n) + \int d^2 r_1 \int d^2 r_2 \mathcal{G}_{11}^{(0)}(\mathbf{r}, \mathbf{r}_1; \omega_n)\mathcal{V}(\mathbf{r}_1, \mathbf{r}_2)\widetilde{\mathcal{G}}_{11}^{(0)}(\mathbf{r}_2, \mathbf{r}'; \omega_n),$$
(6)

where the Green's functions matrix in the absence of the impurity potential satisfies:

$$[(i\hbar\omega_n - \widehat{\xi})\sigma_0 - \sigma_z\mu_B H]\mathcal{G}_{11}^{(0)}(\mathbf{r}, \mathbf{r}'; \omega_n) = \sigma_0\delta(\mathbf{r} - \mathbf{r}').$$
(7)

In attempting to find the desired linear TDGL equation, we focus our attention on the pairing self-consistency equation, to first order in the pair-potential expansion. In terms of the Nambu 2×2 anomalous Green's functions matrix, this equation takes the form:

$$\mathrm{Tr}\langle i\sigma_y\widetilde{\mathcal{G}}_{21}^{(1)}(\mathbf{r}, \mathbf{r}; \tau, \tau)\rangle_{\mathrm{imp}} g = \Delta^*(\mathbf{r}, \tau),$$
(8)

where

$$\langle\widetilde{\mathcal{G}}_{21}^{(1)}(\mathbf{r}, \mathbf{r}; \tau, \tau)\rangle_{\mathrm{imp}} = \int d^2 r'' \int_0^\beta d\tau''\langle\widetilde{\mathcal{G}}_{11}^{(0)T}(\mathbf{r}, \mathbf{r}''; \tau'' - \tau)i\sigma_y\widetilde{\mathcal{G}}_{11}^{(0)}(\mathbf{r}, \mathbf{r}''; \tau'' - \tau)\rangle_{\mathrm{imp}}\Delta^*(\mathbf{r}'', \tau''),$$

$g < 0$ is the BCS coupling constant, and the average is over impurity positions.

Fourier transforming, both spatially and temporally, with wave vector $\mathbf{q}$ and bosonic Matsubara frequency $\Omega_\nu = 2\nu\pi k_B T/\hbar \geqslant 0$, respectively, the self-consistency pairing equation (8) can be transformed (for details see Ref. [32]) into the following frequency and wave number dependent linear GL equation:

$$\ln\left(\frac{T}{T_{c0}}\right) + a_+\psi(1/2 + f_- + x + y)$$
$$+ a_-\psi(1/2 + f_+ + x + y) - \psi(1/2) = 0, \quad (9)$$

where $x \equiv \hbar D q^2/4\pi k_B T$ and $y \equiv \hbar\Omega_\nu/4\pi k_B T$. Here T_{c0} is the mean-field SC transition temperature at zero magnetic field, ψ is the digamma function, $f_\pm = \delta H^2 + \beta \pm \sqrt{\beta^2 - \mu^2 H^2}$, $a_\pm = (1 \pm \beta/\sqrt{\beta^2 - \mu^2 H^2})/2$ are dimensionless functions of the magnetic field H, with the basic parameters: $\beta \equiv \varepsilon_{\mathrm{SO}}/4\pi k_B T$, $\mu \equiv \mu_B/2\pi k_B T$, $\delta \equiv D(de)^2/2\pi k_B T\hbar$, where $D \equiv \hbar E_F/m^*\varepsilon_{\mathrm{SO}}$ is the electron diffusion coefficient.

Note that in the single-band model employed in the above calculations the presence of the spin-orbit interaction does not influence T_{c0}, which is given by the simple BCS expression, $T_{c0} \simeq 2e^\gamma T_D e^{-1/|g|N_{2D}}$, where $\gamma \simeq 0.5772$, and $N_{2D} = m^*/2\pi\hbar^2$ is the single electron DOS. Note also that in Eq. (9) the explicit logarithmic singularity at $T = 0$ is canceled by the asymptotic logarithmic divergence of the digamma function for $T \to 0$, a result equivalent to the removal of the Cooper singularity by finite magnetic field or/and by $\Omega_\nu > 0$.

To take into account the effect of the spin-orbit induced band mixing [18,24], we replace the constant N_{2D} with a minimal model of piecewise DOS function $N_{2D}(E)$, consisting of a relatively heavy, high energy, electron band with DOS, $m^*/2\pi\hbar^2$, and a lighter, low energy, electron band, separated by an energy interval $\sim\varepsilon_{\mathrm{SO}}$, in which $N_{2D}(E) \equiv (m^*/2\pi\hbar^2)\nu(E)$ interpolates between the two pieces (see Fig. 1).

The self-consistency pairing equation (9) enables us to evaluate the wave number and frequency dependent

Cooper-pair fluctuation propagator: $D(q, \Omega_\nu)$. The static $(\Omega_\nu = 0)$ propagator $D(q, \Omega_\nu = 0) \equiv 1/N_{2D}(E_F)\Phi(x; \varepsilon_H)$ can be written in terms of the well-known function of the dimensionless fluctuation kinetic energy variable $x \equiv \hbar D q^2 / 4\pi k_B T$ [20]:

$$\Phi(x; \varepsilon_H) = \varepsilon_H + a_+[\psi(1/2 + f_- + x) - \psi(1/2 + f_-)]$$
$$+ a_-[\psi(1/2 + f_+ + x) - \psi(1/2 + f_+)] \quad (10)$$

and the Gaussian critical shift parameter:

$$\varepsilon_H \equiv \ln\left(\frac{T}{T_{c0}}\right) + a_+ \psi\left(\frac{1}{2} + f_-\right) + a_- \psi\left(\frac{1}{2} + f_+\right) - \psi(1/2). \quad (11)$$

The parameter ε_H should be corrected due to interaction between fluctuations [33]. The correction can be evaluated analytically from the cubic term of the GL equation introduced in Appendix A and is given by [see Eq. (A13)]: $\alpha F(H)\eta(H) \int_0^{x_c} dx/\Phi(x; \varepsilon_H)$, where

$$\alpha \equiv 1/\hbar \pi^3 D N_{2D}(E_F) \quad (12)$$

and $x_c \equiv \hbar D q_c^2 / 4\pi k_B T$. The cutoff wave number q_c typically satisfies $x_c < 1$, so that one may exploit the linear approximation $\Phi(x; \varepsilon_H) = \varepsilon_H + \eta(H)x$, where

$$\eta(H) = a_+ \psi'\left(\frac{1}{2} + f_-\right) + a_- \psi'\left(\frac{1}{2} + f_+\right). \quad (13)$$

The Hartree self-consistent field (SCF) approximation amounts to replacing ε_H, appearing in the interaction correction, with the "dressed" critical shift parameter $\widetilde{\varepsilon}_H$, leading to the SCF equation:

$$\widetilde{\varepsilon}_H \simeq \varepsilon_H + \alpha F(H) \ln\left(1 + \frac{\eta(H)x_c}{\widetilde{\varepsilon}_H}\right), \quad (14)$$

where the logarithmic factor is obtained from the integral over x by using the linear approximation of $\Phi(x; \widetilde{\varepsilon}_H)$, and the field distribution function of the interaction $F(H)$ is given by the Matsubara sum [see Eq. (A14)]:

$$F(H) = \frac{1}{\eta(H)} \sum_{n=0}^{\infty} \frac{\varkappa_n(\varkappa_n^2 + \mu^2 H^2)}{[\varkappa_n(\varkappa_n - 2\beta) + \mu^2 H^2]^3}, \quad (15)$$

where $\varkappa_n = n + 1/2 + 2\beta + \delta H^2$. Equation (14) has no solution with $\widetilde{\varepsilon} \leqslant 0$ (see Ref. [33]), indicating the absence of a genuine SC phase transition due to the interaction between fluctuations. Indeed, as shown in Fig. 3, all solutions of the SCF equation (14) satisfy $\widetilde{\varepsilon}_h > 0$, implying that the critical divergence of the free fluctuations propagator is strictly removed. This also eliminates the critical divergence from both the Aslamazov-Larkin (AL) and the suppressed normal-state conductivities (see below).

III. QUANTUM FLUCTUATIONS AT LOW TEMPERATURES

For temperatures above T_c, the magnetic sheet resistance (MSR), calculated by considering only thermal fluctuations (see Sec. IV for details), accounts quantitatively well for the experimental MSR data reported in Ref. [2] (see Fig. 2). However, in the low temperatures regime well below T_c, large deviations between the calculated and measured MSR data are seen, with the calculated MSR peak quickly narrowing
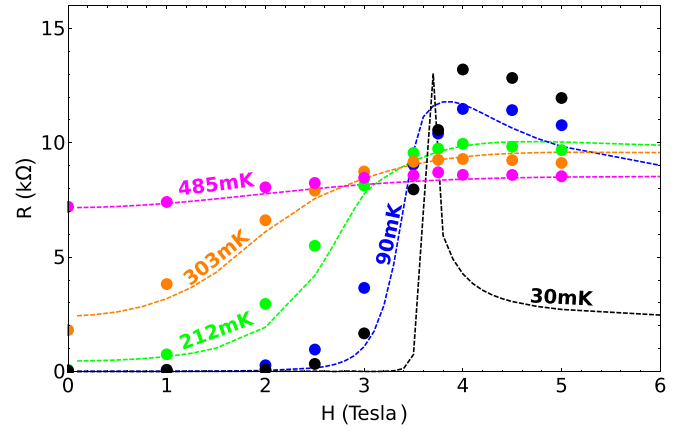

FIG. 2. Calculated sheet resistance as a function of field H for different temperatures, obtained within the framework of the thermal fluctuations theory in the SCF approximation (dashed lines, with temperature labels), plotted together with the corresponding experimental data (full circles) extracted from [2]. The gate voltage V_g employed corresponds to $R_N = 7.5$ kΩ (zero-field sheet resistance at $T = 1$ K). The fitting parameters used are: $T_{c0} = 0.4$ K, $\beta_0 = 8$, $\alpha = 0.1$, $\widetilde{\delta}_0 = 0.028$ (see Appendix B).

upon decreasing temperature, as compared to the rather broad experimental MSR peak. This discrepancy is due to the fact that at low temperatures $\widetilde{\varepsilon}_H$, determined by Eq. (14), is not significantly different from ε_H in the vicinity of the critical point $\varepsilon_H = 0$. The reason, as illustrated by Fig. 3, is in the progressive narrowing of $F(H)$ [Eq. (15)] upon decreasing temperature, having too small tail intensity in the vicinity of the free-fluctuations critical field.

We argue that the observed broadening at very low temperatures is due to quantum fluctuations effect similar to the quantum phase slips reported for SC nanowires [34–37], a phenomenon which was also reported for ultrathin granular SC film [38,39]. We invoke a phenomenological approach describing dynamical tunneling of Cooper pairs through energy barriers, separating SC puddles [40], on equal footing with thermal activation across the same barriers. Thus,
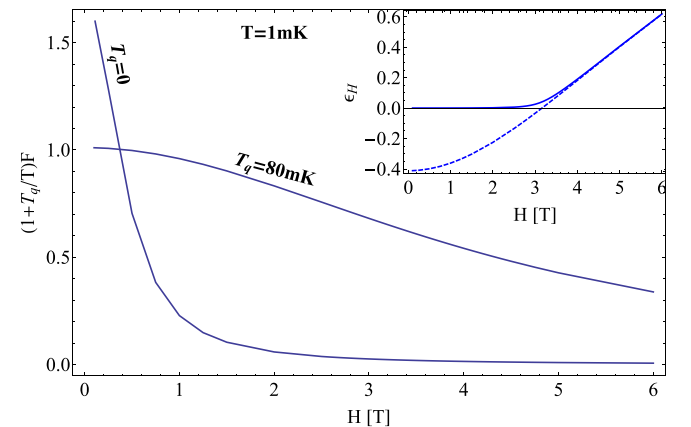

FIG. 3. The field distribution function $(1 + T_Q/T)F_U(H)$, calculated at $T = 1$ mK for $T_Q = 0$ and $T_Q = 80$ mK. Inset: "Bare," ε_H (dashed line), and "dressed," $\widetilde{\varepsilon}_H$ (solid line), critical shift parameters, calculated at $T = 1$ mK and $T_Q = 80$ mK.

we introduce a unified quantum-thermal (QT) fluctuations partition function:

$$Z_{\text{fluct}}^U = \prod_{\mathbf{q}} \int \mathcal{D}\Delta_q \mathcal{D}\Delta_q^* e^{-\frac{\tau_U}{\hbar}\left[\widetilde{\varepsilon}_H^U + \frac{\eta_U(H)\hbar}{4\pi k_B T}Dq^2\right]|\Delta_q|^2 N_{2D}(E_F)},$$

where $1/\tau_U$ is the combined QT attempt rate, defined by: $\hbar/\tau_U \equiv k_B T + \hbar/\tau_Q$, with $1/\tau_Q = k_B T_Q/\hbar$ the tunneling attempt rate [$\widetilde{\varepsilon}_H^U$, and $\eta_U(H)$ will be defined below]. The corresponding Gaussian, unified QT-fluctuations propagator is given by: $D_U(q;\varepsilon_H^U) = k_B(T + T_Q)/N_{2D}(E_F)$ $(\varepsilon_H^U + \frac{\hbar Dq^2 \eta_U(H)}{4\pi k_B T})$.

The inherent dynamics of the quantum tunneling of Cooper-pair fluctuations is introduced to the equilibrium Gorkov-GL functional integral through imaginary time [41]. Consistency requires that the introduction of an excess quantum-tunneling "temperature," T_Q, into the unified QT fluctuation propagator, should be complemented by introduction of a bosonic excitation Matsubara frequency shift $\Omega_\nu/2 = \pi k_B T_Q/\hbar$ into the definitions of the electron-pairing functions $F_U(H)$, ε_H^U, $\eta_U(H)$, under summation over the fermionic Matsubara frequency $\omega_n = (2n+1)\pi k_B T/\hbar$. Thus, one evaluates these unified QT functions from the respective thermal functions: $F(H)$, ε_H, $\eta(H)$, by introducing the shift $n \to n + T_Q/2T$ under the summations over n in Eq. (15) and by shifting the argument of the digamma function and its derivative with the same additive constant $T_Q/2T$ in Eqs. (11) and (13), respectively. The corresponding unified Hartree SCF equation (14) reads: $\widetilde{\varepsilon}_H^U = \varepsilon_H^U + \alpha F_U(H)(1 + T_Q/T)\ln(1 + \frac{x_c\eta_U(H)}{\widetilde{\varepsilon}_H^U})$.

IV. SHEET CONDUCTANCE UNDER PARALLEL MAGNETIC FIELD

A. Fluctuation paraconductivity

In the calculation of the paraconductivity we adopt a modified version of the formalism developed by Fulde and Maki [20] for calculating the AL contribution [22]. The method of calculation, which was first proposed by Schmidt [42], exploits the TDGL functional $\mathfrak{L}(\Delta, \mathbf{A})$ of the

order parameter $\Delta(\mathbf{r}, t)$ and the vector potential $\mathbf{A}(\mathbf{r}, t)$, to find the Cooper-pairs current density:

$$\mathbf{j}(\mathbf{r}, t) = \frac{\partial \mathfrak{L}(\Delta(\mathbf{r}, t), \mathbf{A}(\mathbf{r}, t))}{\partial \mathbf{A}(\mathbf{r}, t)}. \tag{16}$$

A key ingredient in this approach is the inverse fluctuation propagator (in wave-vector-frequency representation) $D^{-1}(\mathbf{q}+2e\mathbf{A}/\hbar, \omega)$, mediating between the order parameter and the GL functional. In the Gaussian approximation, inherent to the Fulde-Maki approach, the relation is quadratic, i.e.:

$$\mathfrak{L}(\Delta, \mathbf{A}) = \left(\frac{1}{2\pi}\right)^2 \int d^2q \left(\frac{1}{2\pi}\right) \int d\omega$$
$$\times |\Delta(\mathbf{q}, \omega)|^2 D^{-1}(\mathbf{q}+2e\mathbf{A}/\hbar, \omega)$$

and the AL time-ordered correlator is given by:

$$Q_{\text{AL}}(i\Omega_\nu)$$
$$= (4eN_{2D}D)^2 d\left(\frac{1}{2\pi}\right)^2 \int d^2q k_B T \sum_{\mu=-\infty}^{\infty}$$
$$\times q_x^2 C(q, \Omega_\mu + \Omega_\nu)D(q, \Omega_\mu + \Omega_\nu)C(q, \Omega_\mu)D(q, \Omega_\mu), \tag{17}$$

where $\Omega_\mu = 2\mu k_B T/\hbar$, $\Omega_\nu = 2\nu k_B T/\hbar$, $\mu = 0, \pm1, \pm2, ...,$ $\nu = 0, 1, 2, ...$ are bosonic Matsubara frequencies. Here the electrical current is generated along the x axis, q_z, q_x are the fluctuation (in-plane) wave-vector components along the magnetic and electric field directions, respectively, $q^2 \equiv q_z^2 + q_x^2$, and $C(\widetilde{q}, \Omega_\mu) \equiv [\partial D^{-1}(\widetilde{q}, \Omega_\mu)/\partial A_x]/4DeN_{2D}\widetilde{q}_x$, with $\widetilde{q} = |\widetilde{\mathbf{q}}|$, $\widetilde{\mathbf{q}} \equiv \mathbf{q} + 2e\mathbf{A}/\hbar$. Note that in Eq. (17) we use for both $C(q, \Omega_\mu)$ and $D(q, \Omega_\mu)$ the notations employed in Sec. I for the fluctuation propagator, where the orbital magnetic field effect is implicitly included, whereas in the above definition of $C(\widetilde{q}, \Omega_\mu)$ it is explicit. A simple calculation yields: $C(q, \Omega_\mu) = \eta(x, y; H)/4\pi k_B T$, where $\eta(x, y; H)$ is obtained from $\eta(H)$, defined in Eq. (13), by replacing $f_\pm$ with $f_\pm + x + y$. Thus, performing the summation over the bosonic Matsubara frequency Ω_μ in Eq. (17) and the analytic continuation $i\Omega_\nu \to \omega + i\delta$, the retarded correlator $Q_{\text{AL}}^R(\omega)$ can be written in the form:

$$Q_{\text{AL}}^R(\omega) = k_B T \left(\frac{2e}{\hbar}\right)^2 \left(\frac{1}{2\pi d}\right) \int_0^\infty x\,dx \sum_{n=0,\pm1,\pm2,....} \frac{\Phi'(x+|n+y|;\widetilde{\varepsilon}_h)}{\Phi(x+|n+y|;\widetilde{\varepsilon}_h)} \frac{\Phi'(x+|n|;\widetilde{\varepsilon}_h)}{\Phi(x+|n|;\widetilde{\varepsilon}_h)}, \tag{18}$$

where $y = \frac{i\hbar\omega}{2\pi k_B T}$, and:

$$\Phi(x+y;\widetilde{\varepsilon}_h) \equiv \widetilde{\varepsilon}_h + a_+(h)[\psi(1/2 + f_-(h) + x + y) - \psi(1/2 + f_-(h))]$$

$$+ a_-(h)[\psi(1/2 + f_+(h) + x + y) - \psi(1/2 + f_+(h))].$$

Using Eq. (18) the desired static sheet conductivity is readily calculated to be:

where $G_0 = e^2/\pi\hbar$ is the conductance quantum. Thus, within the unified QT fluctuations approach, the static AL sheet conductivity is given by:

$$\sigma_{AL}d = \frac{1}{4}\left(\frac{G_0}{\pi}\right)\int_0^\infty \left(\frac{\Phi'(x;\widetilde{\varepsilon}_h)}{\Phi(x;\widetilde{\varepsilon}_h)}\right)^2 dx \tag{19}$$

$$\sigma_{AL}^U d = \left(1 + \frac{T_Q}{T}\right)\frac{1}{4}\left(\frac{G_0}{\pi}\right)\int_0^\infty \left(\frac{\Phi_U'(x;\widetilde{\varepsilon}_H^U)}{\Phi_U(x;\widetilde{\varepsilon}_H^U)}\right)^2 dx, \tag{20}$$

where $\Phi_U(x; \widetilde{\varepsilon}_H^U)$ is obtained from Eq. (10) by replacing $\widetilde{\varepsilon}_H$ with $\widetilde{\varepsilon}_H^U$, and by shifting the argument of all the digamma functions in Eq. (10) with the additive constant $T_Q/2T$.

B. Cooper-pair fluctuations suppressed normal state conductivity

The idea, first exploited by Larkin and Varlamov [43] for the zero field case, is to replace the electron number density N_e in the simple Drude formula for the conductivity $\sigma = N_e e^2 \tau/m^*$, with the number density of electrons occupying quasiparticle states minus the number density ΔN_e of electrons paired into SC puddles. Since $\Delta N_e = 2n_s$, where n_s is the number density of Cooper pairs in SC puddles, the corresponding correction to the Drude conductivity is given by: $\delta\sigma_{\mathrm{DOS}} = -2(n_s e^2/m^*)\tau_{\mathrm{SO}}$. The subscript DOS indicates that this contribution to the conductivity is associated with the suppression of the normal electrons DOS by Cooper-pair fluctuations [44]. The number density, $n_s = (1/d)\int\langle|\psi(q)|^2\rangle d^2q/(2\pi)^2$ [43], is obtained from the superfluid momentum distribution function

$$\langle|\psi(q)|^2\rangle \simeq 2E_F/\pi^2 k_B T \, \Phi(x; \widetilde{\varepsilon}_H) \qquad (21)$$

so that:

$$\delta\sigma_{\mathrm{DOS}} d \simeq -4(G_0/\pi) \int_0^{x_c} dx/\Phi(x; \widetilde{\varepsilon}_H). \qquad (22)$$

The unified QT fluctuations version of the DOS conductivity can be derived by introducing quantum fluctuations into the superfluid momentum distribution function as follows: $2E_F/\pi^2 k_B T \, \Phi(x; \widetilde{\varepsilon}_H) \to 2E_F/\pi^2 k_B(T + T_Q)\Phi_U(x; \widetilde{\varepsilon}_H^U)$, resulting in the following expression:

$$\delta\sigma_{\mathrm{DOS}}^U d \simeq -4\left(\frac{G_0}{\pi}\right) \int_0^{x_c} \frac{dx}{\left(1 + \frac{T_Q}{T}\right)\Phi_U\left(x; \widetilde{\varepsilon}_H^U\right)}. \qquad (23)$$

The *quantum limit* of the sheet conductivity, i.e., the $T \to 0$ limit of $\sigma_{\mathrm{AL}}^U + \delta\sigma_{\mathrm{DOS}}^U$, should be carefully checked to ensure that they are physically meaningful at very low temperatures. It has been shown, indeed (see Ref. [32]), that both σ_{AL}^U and $\delta\sigma_{\mathrm{DOS}}^U$ have well defined quantum ($T \to 0$) limit.

It is important to note that the phenomenological approach, based on the simple Drude formula, used above in deriving Eq. (22) for the DOS conductivity, is to a good approximation equivalent to the result derived by Larkin-Varlamov [43] by means of a fully microscopic (diagrammatic) approach in the dirty limit. For the sake of simplicity of the comparison we show it here by neglecting the interaction between fluctuations and considering the zero field case. In the phenomenological approach we use in the Drude formula: $\delta\sigma^{\mathrm{DOS}} = -2n_s e^2 \tau_{\mathrm{SO}}/m^*$, the fluctuation Cooper-pair density $n_s = d^{-1}(2\pi)^{-2} \int d^2q \langle|\psi(q)|^2\rangle$, with the appropriate form of Eq. (21) for the momentum distribution function:

$$\langle|\psi(q)|^2\rangle = \left(\frac{2E_F}{\pi^2 k_B T}\right) \frac{1}{\varepsilon + \frac{\hbar D}{4\pi k_B T}q^2} \qquad (24)$$

where $\varepsilon = \ln(T/T_{c0})$.

Performing the integration: $n_s = \frac{1}{d}\frac{1}{\hbar D}(\frac{2E_F}{\pi^2})\int_0^{x_c} dx \frac{1}{\varepsilon+x}$ the DOS conductivity is:

$$\delta\sigma^{\mathrm{DOS}} d \simeq -0.4\left(\frac{e^2}{\hbar}\right)\ln\left(\frac{x_c}{\varepsilon}\right). \qquad (25)$$

The corresponding result of the microscopic calculation, which includes all diagrams contributing to the DOS conductivity [43], can be written as:

$$\delta\sigma_{xx}^{\mathrm{DOS}} \simeq -\frac{e^2}{2d\hbar}\kappa(k_B T \tau/\hbar)\ln\left(\frac{x_c}{\varepsilon}\right).$$

In the dirty limit, $k_B T \ll \hbar/\tau$, $\kappa(k_B T \tau/\hbar) \to 56\zeta(3)/\pi^4 \simeq 0.7$, and:

$$\delta\sigma^{\mathrm{DOS}} d \simeq -0.35\left(\frac{e^2}{\hbar}\right)\ln\left(\frac{x_c}{\varepsilon}\right) \qquad (26)$$

in good agreement with Eq. (25).

V. COMPARISON WITH THE EXPERIMENT

Combining all contributions to the sheet conductivity, Eqs. (20) and (23), including the normal-state conductivity σ_n, we have:

$$\sigma^U d = \sigma_n d + \sigma_{\mathrm{AL}}^U d + \delta\sigma_{\mathrm{DOS}}^U d. \qquad (27)$$

Determination of the normal-state conductivity σ_n can reflect on the strong negative MR reported in Ref. [17] for temperatures well above the SC transition. Thus, in our fitting procedure we assume a field-dependent normal state conductivity contribution $\sigma_n(H, T)$, which produces negative MR similar to that observed in Ref. [17], by employing the quadratic function: $\sigma_n(H, T) = \sigma_0 + \sigma_0(H/H_n(T))^2$, with two adjustable parameters σ_0, $H_n(T)$, where the latter is temperature dependent. Employing an extensive fitting procedure, as described in detail in Appendix B, the resulting calculated MSR, best fit to the experimental data sets [2], are shown in Fig. 4. Very good quantitative agreement between the calculated and measured data is seen for the entire data presented. The decreasing magnitudes of the normal-state MR curves, shown in Fig. 4, with increasing temperature are seen to be in qualitative agreement with the experimental negative MR data, presented in Ref. [17] for temperatures well above T_c.

As explained in Ref. [2], since labeling each data set according to the measured gate voltage V_g is not a unique procedure, they are instead labeled by R_N—the corresponding sheet resistance measured at zero field and sufficiently high temperature ($T = 1$ K). The best fitting carrier density $n_{2\mathrm{D}}(R_N)$ ($\sim 0.5 \times 10^{13}$ cm^{-2}) and band effective mass $m^* \simeq 1.6m_e$ are found in good quantitative agreement with the carrier density and cyclotron mass, respectively, extracted from Shubnikov-de Haas (SdH) oscillations measurements reported in Ref. [24]. Note that the above value of $n_{2\mathrm{D}}(R_N)$, as extracted in our fitting, is a small fraction of the measured inverse Hall coefficient $e/R_H \equiv n_{2\mathrm{D}}^{\mathrm{Hall}}(R_N)$ reported in Ref. [2] ($\sim 10^{14}$ cm^{-2}). The situation is quite similar to that reported for the LaAlO$_3$/SrTiO$_3$ (001) interface (see Refs. [45,46]). The large difference between the carrier densities extracted from the two methods was attributed [24,47] to contributions to transport of at least two bands with greatly different mobilities, a band contributing minority carriers with high mobility,
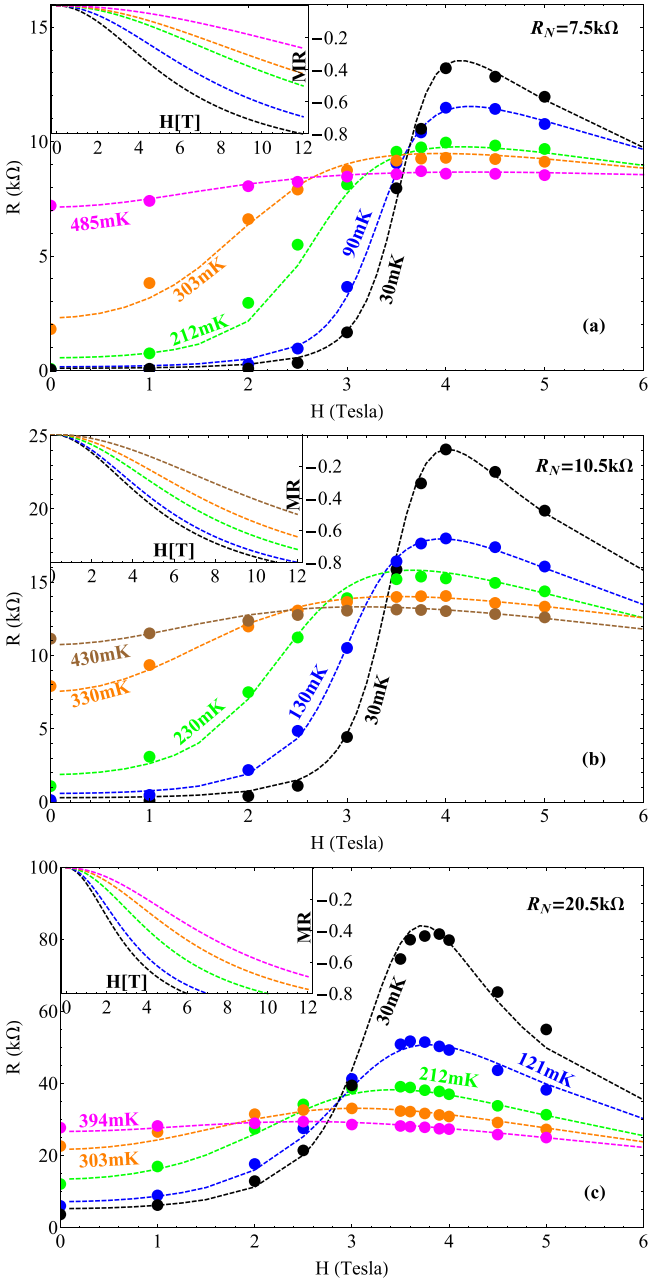
FIG. 4. Calculated sheet resistance as a function of field H for $R_N = 7.5$ kΩ (a), $R_N = 10.5$ kΩ (b), and $R_N = 20.5$ kΩ (c), for different temperatures (dashed lines), plotted together with the corresponding experimental data (full circles) extracted from Ref. [2]. The temperature T used in each curve is labeled. Insets: The normal-state MR curves extracted in the fitting process for each R_N value. Temperatures follow those of the respective main figures, in increasing order with the decreasing magnitude of the MR. The corresponding values of $T_Q(T)$ can be found in Table II. Note the dramatic appearance of resistance at low fields in panel (c) resulting from quantum tunneling effect enhanced by the sharply decreasing electronic DOS.

dominating the SdH oscillations and superconductivity, and majority-carriers band with low mobility, which dominate the Hall resistance.

The key parameter in our theory is the fluctuations-interaction parameter $\alpha(R_N)$, which depends on the normal-state sheet resistance parameter R_N, through $N_{2D}(E_F)$ [see Eq. (12)]. For the values of R_N, presented in Fig. 4, $\alpha(R_N)$ shows a moderate rise upon increasing R_N from 7.5 kΩ to 10.5 kΩ and a significantly larger ascent upon increasing R_N from 10.5 kΩ to 20.5 kΩ (see Fig.(1)). This has two important consequences seen in Fig. 4 (see also Appendix B); a large enhancement of the MSR peak at high fields, and strong amplification of the quantum tunneling induced resistance at low fields, which characterizes anomalous metallic behavior [48]. The corresponding negative normal state MR curves, shown in Fig. 4, are seen to exhibit similar enhancements upon increasing R_N, indicating the sharing roles between Cooper-pair (bosonic) fluctuations and (fermionic) quasiparticles in driving the system to insulator. The implication with regard to $N_{2D}(E_F)$ is that, since $N_{2D}(E_F) \propto 1/\alpha(R_N)$, its relatively large drop upon downshifting the Fermi level from $E_F(R_N = 10.5$ k$\Omega)$ to $E_F(R_N = 20.5$ k$\Omega)$ reflects electron transfers between bands of considerable effective mass ratio [24] (see Fig. 1), which is, however, significantly smaller than that calculated for the (001) interface in Refs. [18,19].

The absence of pronounced MSR peak reported experimentally for the (001) interface is attributed to the relatively large DOS at the Fermi energy, see, e.g., the DOS at the upper band edge shown in Ref. [18], that is: $N_{2D}(E_F^0) \approx 0.3 \times 10^{13}$ cm^{-2} meV^{-1}, which is about an order of magnitude larger than our result for the (111) interface at the upper band edge, shown in Fig. 1.

VI. LOCALIZATION IN MESOSCOPIC SUPERCONDUCTING PUDDLES

The sheet-resistance peaks shown in Fig. 4 at high field reflect localization of Cooper-pair fluctuations within mesoscopic puddles created in response to the driving electric force. This can be seen by considering the Cooper-pairs amplitude correlation function (that is proportional to the static fluctuation propagator in real space), namely:

$$g(\boldsymbol{\rho}) \equiv \langle \psi^*(\mathbf{r}) \psi(\mathbf{r} + \boldsymbol{\rho}) \rangle = \left(\frac{1}{2\pi}\right)^2 \int d^2q \langle |\psi(q)|^2 \rangle e^{i\mathbf{q}\cdot\boldsymbol{\rho}}$$

after exploiting Eq. (21) for $\langle |\psi(q)|^2 \rangle$ with the linear approximation of $\Phi(x; \widetilde{\varepsilon}_H)$, i.e.,

$$g(\rho) \simeq \frac{4}{\pi \eta(H)} \left(\frac{\varepsilon_{SO}}{E_F}\right) n_{2D} \int_0^{q_c} \frac{q \, dq}{\xi_H^{-2} + q^2} J_0(q\rho), \quad (28)$$

where

$$\xi_H = \sqrt{\frac{\hbar D}{4\pi k_B T} \frac{\eta(H)}{\widetilde{\varepsilon}_H}} \quad (29)$$

is the fluctuations correlation length.

Note that the corresponding superfluid density: $n_s = g(0) \simeq (2/\pi\eta(H))(\varepsilon_{SO}/E_F) n_{2D} \ln[1 + (q_c\xi_H)^2]$, is spatially uniform, due to the averaging over the fluctuations configurations. The underlying mesoscopic structure is revealed by the correlation function $g(\rho)$. It is proportional to the probability amplitude for Cooper-pair fluctuations at any point $\mathbf{r}$ to propagate a distance ρ from $\mathbf{r}$. Its dependence on ρ has a decaying envelope, modulated by an oscillatory function
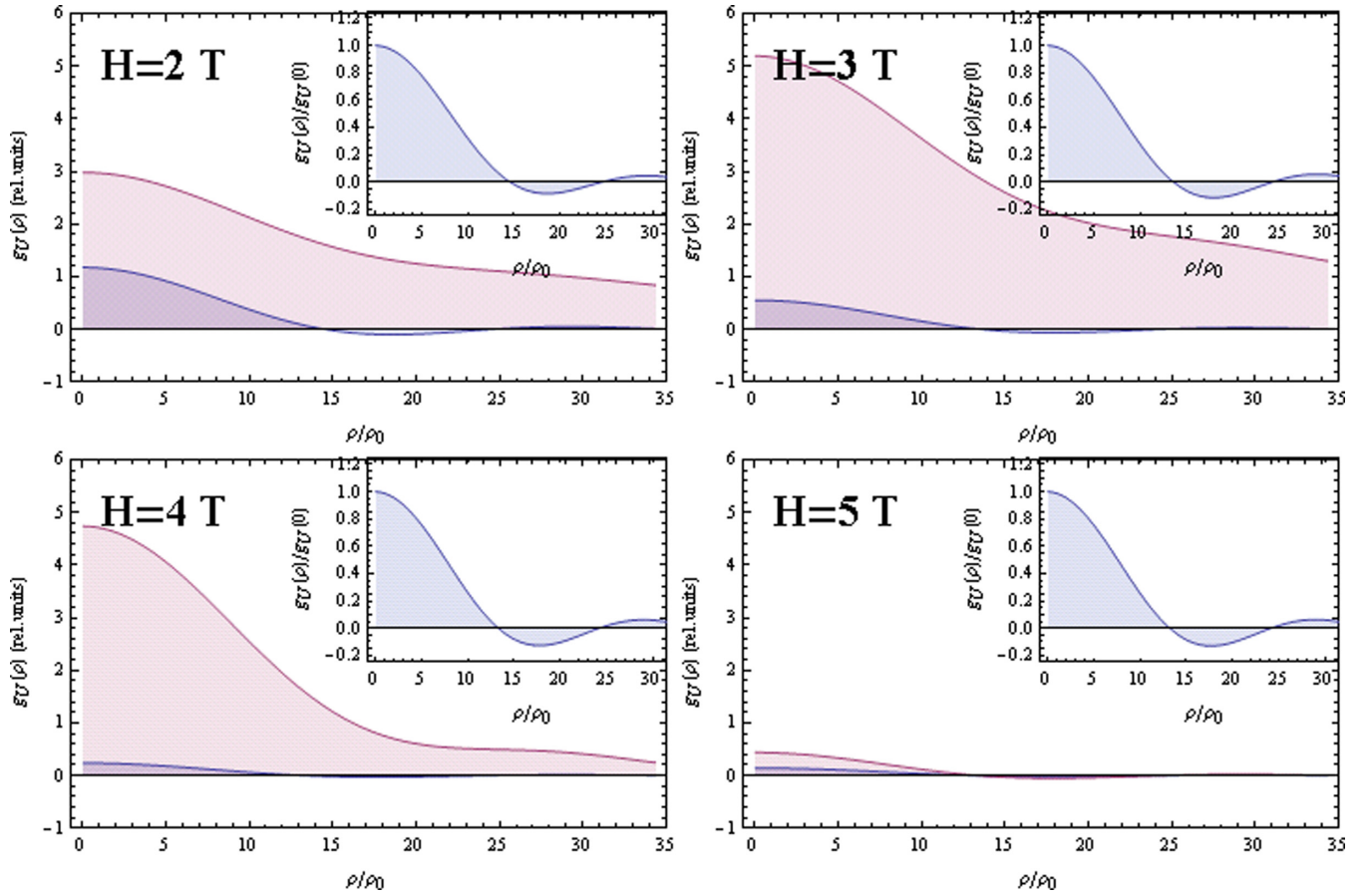
FIG. 5. Blue curves: Fluctuation propagator in real space at a distance ρ (measured in units of ρ_0) from an arbitrary source position, for different fields H, calculated for parameters characterizing Fig. 4(c) with $T_Q = 80$ mK. Brown curves: The same as the blue curves but with $T_Q = 0$. Insets: The fluctuation propagator presented by the blue curves in the main figures, normalized by the respective superfluid densities. Note the apparent saturation of the puddle's size upon increasing the field above $H = 3$ T, which reflects increasing values of $(\xi_h^U)^{-1}$ above the cutoff q_c.

associated with the sharp cutoff q_c (see Fig. 5). The length scale of this attenuation is the correlation length ξ_H [Eq. (29)], which can also be regarded as a length of localization of Cooper-pair fluctuations.

The dependence of ξ_H on the field H is through the interaction-modified critical shift parameter $\widetilde{\varepsilon}_H$ (which also plays the role of an energy gap in the fluctuation spectrum) and the correction factor $\eta(H)$ to the stiffness parameter. Thus, by increasing the field H toward the sheet-resistance peak region, the localization length ξ_H diminishes (see Fig. 5) since the gap $\widetilde{\varepsilon}_H$ increases whereas the stiffness $\eta(H)\hbar D/4\pi k_B T$ decreases (see Fig. 3).

In the presence of quantum tunneling, i.e., for a finite T_Q, $g(\rho) \to g_U(\rho)$:

$$g_U(\rho) \simeq \frac{4(\varepsilon_{\mathrm{SO}}/E_F)n_{2\mathrm{D}}}{\pi(1 + T_Q/T)\eta_U(H)} \int_0^{q_c} \frac{J_0(q\rho)q\,dq}{(\xi_H^U)^{-2} + q^2}, \quad (30)$$

where

$$\xi_H^U = \rho_0 \sqrt{\frac{\eta_U(H)}{\widetilde{\varepsilon}_H^U}} \quad (31)$$

and $\rho_0 \equiv \sqrt{\hbar D/4\pi k_B T}$. Thus, as quantum tunneling of Cooper pairs enhances $\widetilde{\varepsilon}_H$ and diminishes $\eta(H)$, it is

concluded that tunneling shortens the localization length. This also implies diminishing superfluid density due to tunneling (see Fig. 5), which is consistent with the tendency of phase slips to suppress superconducting order.

VII. DISCUSSION

The main message of this paper to the current understanding of the various SIT phenomena is in proposing the concept of suppressed carrier DOS by Cooper-pairs formation as a dominant origin of the insulator side of the SIT. The good quantitative agreement found between the calculated MSR and a very large body of experimental data provided in Ref. [2] supports this proposal. Another important message of this paper (which contrasts the conventional wisdom in this field, see, e.g., a discussion in Ref. [48]) concerns the successful implementation of the AL paraconductivity, generalized to include *self-consistently* the interaction between fluctuations, and the effect of quantum tunneling between SC puddles, *in temperatures range well below the mean-field SC transition*.

The presence of disorder-induced spatial inhomogeneity, in the form of SC islands, which has been extensively discussed in the SIT literature [49–52], is reflected in our approach by the Fourier transform to real space of the fluctuation
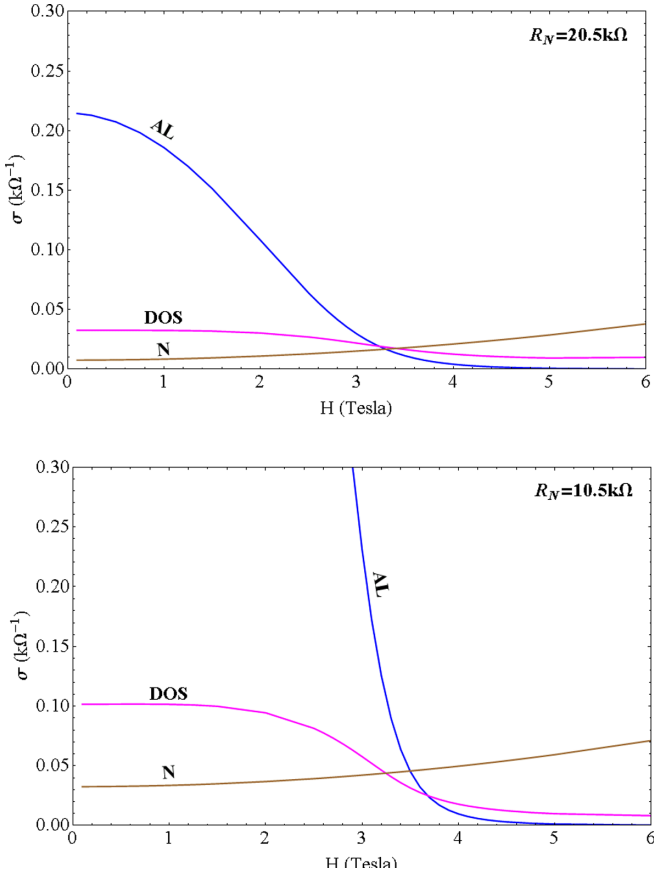
FIG. 6. Upper panel: σ_{AL}, $-\delta\sigma_{\mathrm{DOS}}$, and σ_n contributing to the sheet conductance as functions of field H, calculated with the parameters used in Fig. 4(c), i.e., for $R_N = 20.5$ kΩ ($\alpha = 0.3$). Lower panel: The same as upper panel, calculated with the parameters used in Fig. 4(b), i.e., for $R_N = 10.5$ kΩ ($\alpha = 0.11$). Note the crossing of σ_{AL} and $-\delta\sigma_{\mathrm{DOS}}$ at the onset of the respective MSR peak for each R_N value, shown in Fig. 4.

propagator $D(q; \widetilde{\varepsilon}_H)$, which reveals the underlying structure of mesoscopic SC puddles. The physical picture emerging from analyzing this correlation function is as follows: Upon increasing the magnetic field towards the sheet-resistance peak region the 2D SC fluctuations system breaks into mesoscopic puddles of localized Cooper-pair fluctuations, which consume much of the unpaired mobile electrons dominating the normal state conductivity. The localization arises from enhancement of the energy gap $\widetilde{\varepsilon}_H$ of the fluctuations spectrum and suppres-

sion of their effective stiffness coefficient $\hbar D\eta(H)$ occurring upon increasing magnetic field. In parallel with this localization process upon increasing field, the paraconductivity σ_{AL} decreases more sharply than $-\delta\sigma_{\mathrm{DOS}}$, so that at the point of their crossing (see Fig. 6) one observes the onset of the insulating state, shown in Fig. 4.

However, in this fields range, where the AL conductivity is negligible, and dynamical quantum tunneling diminishes the localized Cooper-pairs puddles, the reinforced conductivity of the unpaired mobile electrons considerably smears the sheet resistance peak developed at very low temperatures. On the other hand, in the low-fields region, where the AL conductivity is dominant, finite resistance is generated (even at zero temperature) by quantum tunneling due to enhanced localization of Cooper pairs in SC puddles.

Notwithstanding the general nature of the proposed mechanism for SIT, the role played by spin-orbit scattering in this system is found quite unique: It strongly mixes relatively heavy electron bands with a lighter electron band and so sharply suppresses the effective DOS upon downshifting the chemical potential across a Lifshitz point. The latter effect is associated with strong enhancement of interaction between Cooper-pair fluctuations, which at low temperatures, significantly enhances the sheet resistance peak at high fields and strongly amplifies the vanishing resistance in the low fields region [48].

APPENDIX A: INTERACTION BETWEEN FREE (GAUSSIAN) FLUCTUATIONS

Interactions between free (Gaussian) fluctuations are introduced by taking into account higher-order terms in the pair-potential expansion of Eq. (4). The leading-order contribution to the interaction is the cubic term in this expansion obtained by substituting the first order term to Eq. (3) and then back to Eq. (4). Exploiting the Hartree decoupling amounts to linearization of the cubic term resulting in the following correction to $\mathcal{G}_{21}$:

$$\delta\mathcal{G}_{21}^{(3)}(\mathbf{r}, \mathbf{r}'; \tau, \tau') \equiv \mathcal{G}_{21}^{(3)}(\mathbf{r}, \mathbf{r}'; \tau, \tau') - \mathcal{G}_{21}^{(1)}(\mathbf{r}, \mathbf{r}'; \tau, \tau') \quad \text{(A1)}$$

with:

$$\delta\mathcal{G}_{21}^{(3)}(\mathbf{r}, \mathbf{r}'; \tau, \tau') = \int d^2r'' \int_0^\beta d\tau'' \int d^2r_1 \int_0^\beta d\tau_1 \int d^2r_2 \int_0^\beta d\tau_2$$
$$\times \mathcal{G}_{11}^{(0)T}(\mathbf{r}, \mathbf{r}''; \tau'' - \tau) i\sigma_y^{(0)} \mathcal{G}_{11}^{(0)}(\mathbf{r}_1, \mathbf{r}''; \tau'' - \tau_1) i\sigma_y \mathcal{G}_{11}^{(0)T}(\mathbf{r}_1, \mathbf{r}_2; \tau_2 - \tau_1) i\sigma_y \mathcal{G}_{11}^{(0)}(\mathbf{r}', \mathbf{r}_2; \tau_2 - \tau')$$
$$\times [k_B T D(\mathbf{r}'' - \mathbf{r}', \tau'' - \tau')\Delta^*(\mathbf{r}_2, \tau_2) + k_B T D(\mathbf{r}_2 - \mathbf{r}_1, \tau_2 - \tau_1)\Delta^*(\mathbf{r}'', \tau'')], \quad \text{(A2)}$$

where $\langle\Delta^*(\mathbf{r}_2, \tau_2)\Delta(\mathbf{r}_1, \tau_1)\rangle = k_B T D(\mathbf{r}_2 - \mathbf{r}_1, \tau_2 - \tau_1) \equiv D_T(\mathbf{r}_2 - \mathbf{r}_1, \tau_2 - \tau_1)$ and $D(\mathbf{r}_2 - \mathbf{r}_1, \tau_2 - \tau_1)$ is the free (Gaussian) fluctuation propagator, whose spatial-temporal Fourier transform, extracted from Eq. (9), is given by:

$$D(q, \Omega_\nu)^{-1} = N_{2D} \begin{bmatrix} \ln(T/T_{c0}) + a_+ \psi(1/2 + f_+ + x + y) \\ + a_- \psi(1/2 + f_- + x + y) - \psi(1/2) \end{bmatrix}. \quad \text{(A3)}$$

The corresponding corrected self-consistency pairing equation in the momentum-energy domain is given by:

$$\int d^2r e^{-i\mathbf{q}\cdot\mathbf{r}} \int_0^\beta d\tau e^{i\Omega_\nu \tau} \left[\begin{array}{c} \text{Tr}\langle i\sigma_y \widetilde{\mathcal{G}}_{21}^{(1)}(\mathbf{r},\mathbf{r};\tau,\tau)\rangle_{\text{imp}} \\ +\text{Tr}\langle i\sigma_y \delta\mathcal{G}_{21}^{(3)}(\mathbf{r},\mathbf{r};\tau,\tau)\rangle_{\text{imp}} \end{array} \right] g = \Delta^*(\mathbf{q},\Omega_\nu) \tag{A4}$$

with the kernel $\delta\widetilde{\mathcal{S}}^{(3)}$ of the cubic term defined by:

$$\int d^2r e^{-i\mathbf{q}\cdot\mathbf{r}} \int_0^\beta d\tau e^{i\Omega_\nu \tau} \langle \delta\widetilde{\mathcal{G}}_{21}^{(3)}(\mathbf{r},\mathbf{r};\tau,\tau)\rangle_{\text{imp}} \equiv 2\Delta^*(\mathbf{q},\Omega_\nu)N_{2D}\int \frac{d^2q'}{(2\pi)^2}D_T(q')k_BT\sum_{n=-\infty}^\infty \delta\widetilde{\mathcal{S}}^{(3)}(\mathbf{q},\mathbf{q}';\omega_n,\Omega_\nu-\omega_n), \tag{A5}$$

where $D_T(q')\equiv k_BTD(q',0)$. Now, the crucial importance of the correction term is near the vanishing of the "bare" linear term at the critical point, where $q=0$, $\Omega_\nu=0$. Thus, exploiting also the critical divergence of $D_T(q')$ at $q'=0$, the dependence of the electronic kernel $\delta\widetilde{\mathcal{S}}^{(3)}$ on the very small wave vectors $\mathbf{q}$, $\mathbf{q}'$ and frequency Ω_ν of the fluctuations can be safely neglected, so that in Eq. (A5) one may assume that: $\delta\widetilde{\mathcal{S}}^{(3)}(\mathbf{q},\mathbf{q}';\omega_n,\Omega_\nu-\omega_n) \approx \delta\widetilde{\mathcal{S}}^{(3)}(\mathbf{q}=\mathbf{0},\mathbf{q}'=0;\omega_n,-\omega_n) \equiv \delta\widetilde{\mathcal{S}}^{(3)}(\omega_n)$ and rewrite it in the form:

$$\int d^2r e^{-i\mathbf{q}\cdot\mathbf{r}} \int_0^\beta d\tau e^{i\Omega_\nu \tau} \langle \delta\widetilde{\mathcal{G}}_{21}^{(3)}(\mathbf{r},\mathbf{r};\tau,\tau)\rangle_{\text{imp}} \approx 2\Delta^*(\mathbf{q},\Omega_\nu)\int \frac{d^2q'}{(2\pi)^2}D_T(q')k_BT\sum_{n=-\infty}^\infty N_{2D}\delta\widetilde{\mathcal{S}}^{(3)}(\omega_n), \tag{A6}$$

where the undressed kernel, i.e., prior to inserting the self-energy and vertex corrections, is given by:

$$N_{2D}\delta\mathcal{S}^{(3)}(\omega_n) = \int \frac{d^2p}{(2\pi)^2}\mathcal{G}_{11}^{(0)T}(\mathbf{p},\omega_n)i\sigma_y\mathcal{G}_{11}^{(0)}(-\mathbf{p},-\omega_n)i\sigma_y\mathcal{G}_{11}^{(0)T}(\mathbf{p},\omega_n)i\sigma_y\mathcal{G}_{11}^{(0)}(-\mathbf{p},-\omega_n)$$

with

$$\mathcal{G}_{11}^{(0)}(\mathbf{p},\omega_n) = \begin{pmatrix} G_-^{(0)}(\mathbf{p},\omega_n) & 0 \\ 0 & G_+^{(0)}(\mathbf{p},\omega_n) \end{pmatrix} = \begin{pmatrix} (i\hbar\omega_n-\xi_p-\mu_BH)^{-1} & 0 \\ 0 & (i\hbar\omega_n-\xi_p+\mu_BH)^{-1} \end{pmatrix}$$

$$\delta\mathcal{S}^{(3)}(\omega_n) = \begin{pmatrix} 0 & \delta\mathcal{S}_{\uparrow\downarrow}^{(3)}(\omega_n) \\ \delta\mathcal{S}_{\downarrow\uparrow}^{(3)}(\omega_n) & 0 \end{pmatrix} \equiv \begin{pmatrix} 0 & \delta\mathcal{S}_-^{(3)}(\omega_n) \\ \delta\mathcal{S}_+^{(3)}(\omega_n) & 0 \end{pmatrix}$$

and

$$N_{2D}\delta\mathcal{S}_-^{(3)}(\omega_n) = -\int \frac{d^2p}{(2\pi)^2}G_-^{(0)}(\mathbf{p},\omega_n)G_+^{(0)}(-\mathbf{p},-\omega_n)G_-^{(0)}(\mathbf{p},\omega_n)G_+^{(0)}(-\mathbf{p},-\omega_n),$$

$$N_{2D}\delta\mathcal{S}_+^{(3)}(\omega_n) = \int \frac{d^2p}{(2\pi)^2}G_+^{(0)}(\mathbf{p},\omega_n)G_-^{(0)}(-\mathbf{p},-\omega_n)G_+^{(0)}(\mathbf{p},\omega_n)G_-^{(0)}(-\mathbf{p},-\omega_n).$$

Note the symmetry property of the (singlet pairing) kernel components:

$$\delta\mathcal{S}_+^{(3)}(\omega_n) = -\delta\mathcal{S}_-^{(3)}(\omega_n), \quad Tr[\delta\mathcal{S}^{(3)}(\omega_n)] = \delta\mathcal{S}_{\downarrow\uparrow}^{(3)}(\omega_n) - \delta\mathcal{S}_{\uparrow\downarrow}^{(3)}(\omega_n) = 2\delta\mathcal{S}_+^{(3)}(\omega_n).$$

Inserting impurity scattering corrections, bridging pairing vertices, as well as self-energy corrections, $\omega_n \to \widetilde{\omega}_n = \omega_n + (1/2\tau_{SO})\text{sgn}(\omega_n)$, we have:

$$N_{2D}\delta\widetilde{\mathcal{S}}_{\downarrow\uparrow}^{(3)}(\omega_n) = (|\widetilde{\omega}_n|-iI\text{sgn}(\omega_n))^3 \int \frac{d^2p}{(2\pi)^2}G_{\downarrow\downarrow}^{(0)}(\mathbf{p},\widetilde{\omega}_n)\widetilde{s}_{\downarrow\uparrow}(\omega_n)G_{\uparrow\uparrow}^{(0)}(-\mathbf{p},-\widetilde{\omega}_n)\widetilde{s}_{\uparrow\downarrow}(\omega_n)G_{\downarrow\downarrow}^{(0)}(\mathbf{p},\widetilde{\omega}_n)\widetilde{s}_{\downarrow\uparrow}(\omega_n)G_{\uparrow\uparrow}^{(0)}(-\mathbf{p},-\widetilde{\omega}_n),$$

$$N_{2D}\delta\widetilde{\mathcal{S}}_{\uparrow\downarrow}^{(3)}(\omega_n) = -(|\widetilde{\omega}_n|+iI\text{sgn}(\omega_n))^3 \int \frac{d^2p}{(2\pi)^2}G_{\uparrow\uparrow}^{(0)}(\mathbf{p},\widetilde{\omega}_n)\widetilde{s}_{\uparrow\downarrow}(\omega_n)G_{\downarrow\downarrow}^{(0)}(-\mathbf{p},-\widetilde{\omega}_n)\widetilde{s}_{\downarrow\uparrow}(\omega_n)G_{\uparrow\uparrow}^{(0)}(\mathbf{p},\widetilde{\omega}_n)\widetilde{s}_{\uparrow\downarrow}(\omega_n)G_{\downarrow\downarrow}^{(0)}(-\mathbf{p},-\widetilde{\omega}_n),$$

where $G_{\uparrow\uparrow}^{(0)}(\mathbf{p},\omega_n) \equiv G_-^{(0)}(\mathbf{p},\omega_n)$, $G_{\downarrow\downarrow}^{(0)}(\mathbf{p},\omega_n) \equiv G_+^{(0)}(\mathbf{p},\omega_n)$, and the two possible vertex renormalization factors, $\widetilde{s}_+(\omega_n) \equiv \widetilde{s}_{\downarrow\uparrow}(\omega_n)$, $\widetilde{s}_-(\omega_n) \equiv \widetilde{s}_{\uparrow\downarrow}(\omega_n)$, are given by (see Ref. [32]):

$$\widetilde{s}_\pm(\omega_n) \approx \frac{|\omega_n|+a_H+b\mp iI\text{sgn}(\omega_n)}{(|\omega_n|+a_H)^2-b^2+I^2}, \tag{A7}$$

where $a_H \equiv b+2D(edH/\hbar)^2$, $b \equiv 1/2\tau_{SO}$, and $I \equiv \mu_BH/\hbar$. Thus, we may rewrite now the linearized cubic term in Eq. (A4) in the more explicit form:

$$\int d^2r e^{-i\mathbf{q}\cdot\mathbf{r}} \int_0^\beta d\tau e^{i\Omega_\nu \tau}\text{Tr}\langle i\sigma_y\delta\mathcal{G}_{21}^{(3)}(\mathbf{r},\mathbf{r};\tau,\tau)\rangle_{\text{imp}} \approx 4k_BT(N_{2D}/\hbar^3)\sum_{n=0}^\infty \text{Re}[\widetilde{s}_+(\omega_n)|\widetilde{s}_+(\omega_n)|^2] \int \frac{d^2q'}{(2\pi)^2}D_T(q')\Delta^*(\mathbf{q},\Omega_\nu), \tag{A8}$$

where $\widetilde{s}_+(\omega_n)$ is given in Eq. (A7).

TABLE I. Values of the basic microscopic parameters of the model extracted in the fitting process from the experimental sheet resistance data reported in Ref. [2] for three values of R_N.

R_N (kΩ)	β_0	α	ν (E_F)	ϵ_{SO} (meV)	n_{2D} (cm^{-2})	E_F (meV)
7.5	14	0.09	1.00	3.2	0.55×10^{13}	8.2
10.5	12.5	0.11	0.77	2.87	0.48×10^{13}	7.2
20.5	11	0.30	0.29	2.52	0.43×10^{13}	6.5

We therefore expand $D(q, \Omega_\nu = 0)^{-1}$ [Eq. (A3)] to first order in q^2 to find that:

$$D(q, 0)^{-1} \simeq N_{2D}\left[\varepsilon_H + \frac{\hbar D}{4\pi k_B T}\eta(H)q^2\right], \tag{A9}$$

where the finite-field critical shift parameter ε_H is defined in Eq. (11). The effect of the interaction term near the critical point can be now included in a modified form of Eq. (A9), by using Eq. (A8), i.e.,

$$D_T(q)^{-1}k_B T \simeq N_{2D}\left[\varepsilon_H + \frac{\hbar D}{4\pi k_B T}\eta(H)q^2 + (4k_B T/\hbar^3)\sum_{n=0}^{\infty}\frac{(\omega_n + a_H + b)[(\omega_n + a_H + b)^2 + I^2]}{[(\omega_n + a_H)^2 - b^2 + I^2]^3}\int\frac{d^2q'}{(2\pi)^2}D_T(q')\right]. \tag{A10}$$

The interaction term includes, as a factor, the thermal fluctuation propagator $D_T(q')$, which is proportional to $1/N_{2D}(E_F)$. $D_T(q)$ may be determined by solving numerically the complicated integral equation (A10). A much more practical approach is to use the well-known SCF approximation, employed, e.g., in a similar situation by Ulla and Dorsey in Ref. [23]. In this scheme the third term within the large brackets in Eq. (A10), associated with the linearized cubic term, is absorbed in the field-dependent critical shift parameter ε_H to form the interaction-modified critical shift parameter:

$$\widetilde{\varepsilon}_H \equiv \varepsilon_H + \left(4k_B T/\hbar^3\right)\sum_{n=0}^{\infty}\mathbf{Re}[\widetilde{s}_+(\omega_n)]|\widetilde{s}_+(\omega_n)|^2\int\frac{d^2q'}{(2\pi)^2}D_T(q'), \tag{A11}$$

and then, by considering $D_T(q')$ on the RHS of Eq. (A10) as a function of $\widetilde{\varepsilon}_H$: $D_T(q; \widetilde{\varepsilon}_H) \simeq (k_B T/N_{2D})[\widetilde{\varepsilon}_H + \frac{\hbar D}{4\pi k_B T}q^2\eta(H)]^{-1}$, it can be evaluated by solving Eq. (A11) for $\widetilde{\varepsilon}_H$, after replacing there $D_T(q')$ with $D_T(q'; \widetilde{\varepsilon}_H)$. The resulting equation, determining $\widetilde{\varepsilon}_H$, can be conveniently rewritten in terms of the following dimensionless parameters:

$$\delta_0 \equiv \frac{D(deH_{c\|0}^*)^2}{2\pi k_B T_c^* \hbar}, \quad \mu_0 \equiv \frac{\mu_B H_{c\|0}^*}{2\pi k_B T_c^*}, \quad \beta_0 \equiv \frac{\hbar b}{2\pi k_B T_c^*}, x_0 \equiv \left(\frac{\hbar D q_c^2}{4\pi k_B T_c^*}\right) \tag{A12}$$

and the reduced field and temperature, $h \equiv H/H_{c\|0}^*$, $t \equiv T/T_c^*$, respectively, as

$$\widetilde{\varepsilon}_h = \varepsilon_h + \alpha F(h)\int_0^{x_0 t^{-1}}\frac{dx}{\widetilde{\varepsilon}_h/\eta(h) + x} \simeq \varepsilon_h + \alpha F(h)\ln\left(1 + \frac{\eta(h)x_0}{t\widetilde{\varepsilon}_h}\right), \tag{A13}$$

where α is defined in Eq. (12) in the main text, $T_c^* = 0.212$ K and $H_{c\|0}^* = 4.5$ T are characteristic parameters determining the scales of the SC transition temperature and the critical parallel field (at zero temperature), respectively, and $x_0 \equiv \hbar D q_c^2/4\pi k_B T_c^*$. The function $F(h)$ is obtained from Eq. (A10) and is given by:

$$F(h) = \frac{1}{\eta(h)}\sum_{n=0}^{\infty}\frac{(n + 1/2 + 2\beta + \overline{\delta}h^2)[(n + 1/2 + 2\beta + \overline{\delta}h^2)^2 + \mu^2 h^2]}{[(n + 1/2 + \overline{\delta}h^2)(n + 1/2 + 2\beta + \overline{\delta}h^2) + \mu^2 h^2]^3} \tag{A14}$$

with $\beta = \beta_0/t$, $\mu = \mu_0/t$, and $\overline{\delta} \equiv \delta_0/t$.

APPENDIX B: THE FITTING PROCESS

Focusing on three representative R_N values (see Table I) of the extensive experimental sheet-resistance data reported in Ref. [2], we have exploited the data provided in Ref. [7] to select values for the basic (gate-voltage dependent) microscopic parameters of our theoretical model; $\beta_0(R_N) \equiv \varepsilon_{SO}(R_N)/4\pi k_B T_c^*$ and $\delta_0(R_N) \equiv D(R_N)(deH_{c\|0}^*)^2/2\pi k_B T_c^* \hbar$. The dimensionless Zeeman splitting parameter $\widetilde{I}_0 \equiv \mu_B H_{c\|0}^*/2\pi k_B T_c^*$ was selected to coincide with the free-electron value: $\widetilde{I}_0 = 2.4$. Given the uncertainty involved in determining the numerical

values of $\varepsilon_{SO}(R_N)$ from the current literature, we allow for some freedom in their selection in order to facilitate the fitting process.

The key interaction parameter $\alpha(R_N)$ [see Eq. (12)] is related to $\beta_0(R_N)$ through:

$$\alpha(R_N) = \frac{\alpha_0}{\kappa(R_N)\nu(E_F)}, \tag{B1}$$

where

$$\kappa(R_N) \equiv \frac{\eta_{2D}(R_N)}{\beta_0(R_N)} \tag{B2}$$

$\alpha_0 = 2/\pi^3 = 0.0645$, $\quad \eta_{2D}(R_N) \equiv \hbar^2 n_{2D}(R_N)/4\pi m^* k_B T_c^*$, and $n_{2D}(R_N) = k_F^2/2\pi$ is the effective interface carrier density, with k_F the Fermi wave number.

Another important, gate-voltage dependent parameter is the dimensionless cutoff $x_0 \equiv (T/T_c^*)x_c$. Its evaluation (through q_c) is beyond the scope of our theory, however its dependence on the gate voltage can be expressed through the connecting function $\kappa(R_N)$ [Eq. (B2)], i.e.,

$$x_0(R_N) = \widetilde{x}_0 \kappa(R_N), \tag{B3}$$

where $\widetilde{x}_0 \equiv E_c/2k_B T_c^*$ is a free adjustable parameter (best fitting value: $\widetilde{x}_0 = 0.015$), independent of R_N, with $E_c \equiv \hbar^2 q_c^2/2m^*$. Its value influences mainly the high field behavior through the DOS conductivity, and its optimal selection is closely connected to the selected value of the normal state conductivity parameter σ_n.

A similar dependence on R_N characterizes the dimensionless diamagnetic energy parameter $\delta_0 \equiv (T/T_c^*)\overline{\delta}$, i.e.,

$$\delta_0(R_N) = \widetilde{\delta}_0 \kappa(R_N), \tag{B4}$$

where $\widetilde{\delta}_0 \equiv E_d/2k_B T_c^*$ and $E_d \equiv (deH_{c\|0}^*)^2/m^*$ is the diamagnetic energy, which depends on the effective width of the interface region. The latter contains only a few atomic layers so that $d \sim 1$ nm. The mean-field transition temperature at zero field, T_{c0}, is treated here as an adjustable parameter (best fitting value: $T_{c0} = 0.43$ K) due to the lack of detailed microscopic calculations of the basic SC parameters characterizing the complex LaAlO$_3$/SrTiO$_3$ (111) interface.

The best fitting values of the spin-orbit energy parameter $\varepsilon_{SO}(R_N)$ (see Table I), obtained in our fitting process, decrease monotonically with the decreasing values of the gate voltage V_g (or the increasing values of R_N) on the LHS of the dome-shaped curve of ε_{SO} vs V_g shown in Ref. [7]. The magnitude of the largest fitted value of ε_{SO} (i.e., 3.2 meV at $R_N = 7.5$ kΩ) is by a factor of two smaller than the maximum found in Ref. [7] on the basis of mean-field calculation of the critical field $H_{c\|}$ vs ε_{SO} and its determination vs V_g from resistivity measurements. The differences are likely to be due to the failure of the mean-field approximation in the fluctuation-controlled phenomenon under study.

Thus, examining the sheet-resistance data presented in Ref. [2], we may roughly identify $\varepsilon_{SO}(7.5$ k$\Omega)$ with the top of the dome-shaped ε_{SO} vs V_g curve shown in Ref. [7]. This enables us to start constructing the DOS function $N_{2D}(E)$ from the best fitting parameters $\alpha(R_N)$ [Eq. (B1)] and $\kappa(R_N)$ [Eq. (B2)]. Exploiting Eq. (12) of the main text, one may find $N_{2D}(E_F)$ from the values of $\alpha(R_N)$, provided the

diffusion coefficient D is known. The latter, $D \approx 1.8 \times 10^{-4}$ m^2/s, is found by exploiting the weak antilocalization relation: $eD = \varepsilon_{SO}(R_N)/4H_{SO}(R_N)$ [7] (with H_{SO}–the spin-orbit field, estimated to be about 4.5 T at $R_N = 7.5$ kΩ), and our best fitting value for $\varepsilon_{SO}(7.5$ k$\Omega) \simeq 3.2$ meV. Assuming for the range of the R_N values investigated that $\varepsilon_{SO}(R_N)$ is a linear function of the carrier density $n_{2D}(R_N)$, we have found the best fitting value $\kappa(R_N) \equiv \kappa = 0.8$. These results enable us finding numerical estimates for both the carrier density n_{2D} and the effective mass m^* by solving the consequent coupled equations:

$$\frac{\hbar^2 n_{2D}}{m^* \varepsilon_{SO}} = \kappa = 0.8, \tag{B5}$$

$$\pi \frac{\hbar^3 n_{2D}}{\varepsilon_{SO} m^{*2}} = D = 1.8 \times 10^{-4} \left(\frac{m^2}{s} \right) \tag{B6}$$

yielding $n_{2D}(7.5$ k$\Omega) \simeq 0.55 \times 10^{13}$ cm^{-2}, and $m^* \simeq 1.6 m_e$, where m_e is the free-electron mass.

An independent determination of the effective mass m^*, which provides a self-consistent test of the fitting procedure, can be made by exploiting Eq. (12) with the best fitting values of $\nu(E_F)$ and $\alpha(R_N)$ at $R_N = 7.5$ kΩ, together with the weak antilocalization value of D found above. The resulting equation for m^*, after substituting the best fitting values: $\nu(E_F) = 1$ and $\kappa = 0.8$ in Eq. (B1), reads: $2\hbar/\pi^2 Dm^* = 0.0875$, where $D \approx 1.8 \times 10^{-4}$ m^2/s. The result, $m^* \simeq 1.5 m_e$, agrees quite well with the value found above. It is also found to be in very good agreement with the cyclotron effective mass ($m_c^* = 1.6 m_e$) reported in Ref. [24] using SdH oscillations measurements.

Our next step in constructing the DOS function $N_{2D}(E)$ is to exploit the best fitting values of $\alpha(R_N)$ for the different values of R_N investigated (with $\kappa = 0.8$) in Eq. (B1) and then extract the corresponding values of $\nu(E_F)$ (see Table I). The corresponding values of the carrier density and Fermi energy can be found from the respective relations:

$$n_{2D}(R_N) = 4\pi \frac{m^* k_B T_c^*}{\hbar^2} \kappa \beta_0(R_N), \tag{B7}$$

$$E_F(R_N) = \pi \frac{\hbar^2 n_{2D}(R_N)}{m^*}. \tag{B8}$$

Comparing the results for the carrier density $n_{2D}(R_N)$, shown in Table I, to the data reported in Ref. [2] for the measured inverse Hall coefficient $e/R_H \equiv n_{2D}^{Hall}(R_N)$, we find the former smaller than the latter by one to two orders of

TABLE II. Values of the parameters extracted in the fitting process, which determine the temperature and field dependencies of the normal-state MR and of the quantum tunneling attempt rate T_Q, for the different values of R_N.

$R_N = 7.5$ (kΩ)				$R_N = 10.5$ (kΩ)				$R_N = 20.5$ (kΩ)			
T (mK)	T_q (mK)	H_q (T)	H_n (T)	T (mK)	T_q (mK)	H_q (T)	H_n (T)	T (mK)	T_q (mK)	H_q (T)	H_n (T)
30	78	8	6	30	80	7.3	5.5	30	89	6.5	3
90	70	10	8	130	68	10	6	121	81	7	3.5
212	52	20	12	230	56	15	8	212	72	8	5
303	40	25	14	330	45	18	9	303	60	10	6.5
485	0	30	20	430	22	25	12	394	50	20	8

magnitude. However, the values of $n_{2D}(R_N)$ shown in Table I (i.e., $\sim 0.5 \times 10^{13}$ cm^{-2}) are seen to be in good agreement with the sheet carrier density n_{2D}^{SdH}, determined from the SdH oscillations measurements, reported in Ref. [24]. The large difference between the carrier densities extracted from the two methods could be attributed to contributions to transport of at least two bands with different mobilities (see the main text for the detailed explanation).

The dimensionless diamagnetic energy, $\delta_0(R_N)$, can be used for determining the effective film thickness d in our model, in order to estimate the width of the actual interface. So using the diffusion coefficient $D \approx 1.8 \times 10^{-4}$ m^2/s and our fitting value, $\delta_0(7.5 \text{ k}\Omega) = 0.028(\widetilde{\delta}_0 = 0.035)$, in the above expression for $\delta_0(R_N)$, we find for the film thickness $d \approx 0.8$ nm, which is quite a reasonable result.

The normal-state conductivity contribution $\sigma_n(H, T)$, defined in the main text with the two adjustable parameters σ_0 and $H_n(T)$ (see Table II), can be tested vs the negative MR observed in Refs. [17] and [18]. Using the usual definition of the MR, i.e., $\text{MR}(H, T) \equiv [\rho_n(H, T) - \rho_n(0, T)]/\rho_n(0, T)$, where $\rho_n(H, T) = 1/\sigma_n(H, T)$, our model yields the expression:

$$\text{MR}(H, T) = -\frac{(H/H_n(T))^2}{1 + (H/H_n(T))^2},\qquad (B9)$$

which is plotted in Fig. 4 of the main text for the different R_N values investigated here.

Finally, the large body of experimental data analyzed in this fitting process enables us to determine the temperature and field dependence of the phenomenological quantum tunneling "temperature" parameter $T_Q(T, H)$. For the field
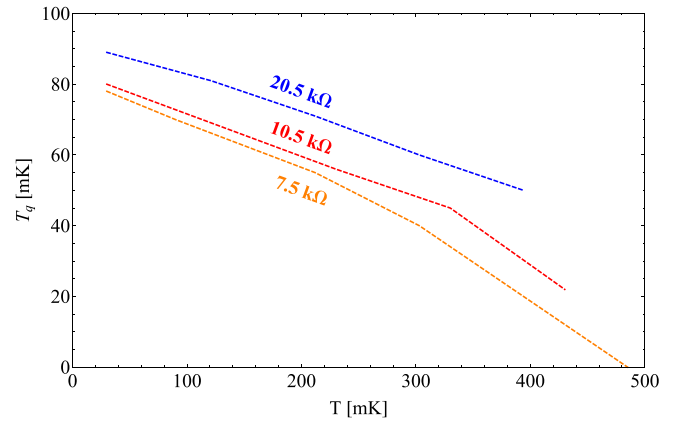

FIG. 7. Tunneling attempt rate T_Q (in mK units) vs T for $R_N = 7.5, 10.5$, and 20.5 kΩ, plotted on the basis of the parameters shown in Table II.

dependence we have selected a particular form, i.e.,

$$T_Q(T, H) = T_Q(T)\left[1 - \left(\frac{H}{H_Q(T)}\right)^2\right],\qquad (B10)$$

which reflects the expected [36] decreasing quadratic dependence of the SC order parameter on increasing field [see Table II for the values of $T_Q(T)$ and $H_Q(T)$]. The temperature dependence at zero field, $T_Q(T)$, for the three values of R_N, is shown in Fig. 7. It is seen to qualitatively follow the expected decreasing order parameter with increasing temperature that would have been measured locally within a superconducting fluctuation puddle. The somewhat larger values of $T_Q(T)$ at larger R_N, which reflect larger tunneling attempt frequency of fluctuations across GL energy barriers, seems to be a reasonable outcome of the respective larger interaction coupling constant α between Gaussian fluctuations.

[1] A. Ohtomo, and H. Y. Hwang, A high-mobility electron gas at the LaAlO$_3$/SrTiO$_3$ heterointerface, Nature (London) **427**, 423 (2004).

[2] M. Mograbi, E. Maniv, P. K. Rout, D. Graf, J.-H. Park, and Y. Dagan, Vortex excitations in the insulating state of an oxide interface, Phys. Rev. B **99**, 094507 (2019).

[3] A. D. Caviglia, S. Gariglio, N. Reyren, D. Jaccard, T. Schneider, M. Gabay, S. Thiel, G. Hammerl, J. Mannhart, and J.-M. Triscone, Electric field control of the LaAlO3/SrTiO3 interface ground state, Nature (London) **456**, 624 (2008).

[4] J. Biscaras, N. Bergeal, S. Hurand, C. Feuillet-Palma, A. Rastogi, R. C. Budhani, M. Grilli, S. Caprara, and J. Lesueur, Multiple quantum criticality in a two-dimensional superconductor, Nat. Mater. **12**, 542 (2013).

[5] M. M. Mehta, D. A. Dikin, C. W. Bark, S. Ryu, C. M. Folkman, C. B. Eom, and V. Chandrasekhar, Magnetic field tuned superconductor-to-insulator transition at the LaAlO$_3$/SrTiO$_3$ interface, Phys. Rev. B **90**, 100506(R) (2014).

[6] S. Davis, Z. Huang, K. Han, Ariando, T. Venkatesan, and V. Chandrasekhar, Magnetoresistance in the superconducting state

at the (111) LaAlO$_3$/SrTiO$_3$ interface, Phys. Rev. B **96**, 134502 (2017).

[7] P. K. Rout, E. Maniv, and Y. Dagan, Link between the Superconducting Dome and Spin-Orbit Interaction in the (111) LaAlO$_3$/SrTiO$_3$ Interface, Phys. Rev. Lett. **119**, 237002 (2017).

[8] D. B. Haviland, Y. Liu, and A. M. Goldman, Onset of Superconductivity in the Two-Dimensional Limit, Phys. Rev. Lett. **62**, 2180 (1989).

[9] A. F. Hebard and M. A. Paalanen, Magnetic-Field-Tuned Superconductor-Insulator Transition in Two-Dimensional Films, Phys. Rev. Lett. **65**, 927 (1990).

[10] A. Yazdani and A. Kapitulnik, Superconducting-Insulating Transition in Two-Dimensional a-MoGe Thin Films, Phys. Rev. Lett. **74**, 3037 (1995).

[11] T. I. Baturina, A. Y. Mironov, V. M. Vinokur, M. R. Baklanov, and C. Strunk, Localized Superconductivity in the Quantum-Critical Region of the Disorder-Driven Superconductor-Insulator Transition in TiN Thin Films, Phys. Rev. Lett. **99**, 257003 (2007).

[12] A. T. Bollinger, G. Dubuis, J. Yoon, D. Pavuna, J. Misewich, and I. Bozovic, Superconductor–insulator transition

in La$_{2-x}$ Sr$_x$CuO$_4$ at the pair quantum resistance, Nature (London) **472**, 458 (2011).

[13] M. Ovadia, D. Kalok, B. Sacepe, and D. Shahar, Duality symmetry and its breakdown in the vicinity of the superconductor–insulator transition, Nat. Phys. **9**, 415 (2013).

[14] M. A. Steiner, G. Boebinger, and A. Kapitulnik, Possible Field-Tuned Superconductor-Insulator Transition in High-Tc Superconductors: Implications for Pairing at High Magnetic Fields, Phys. Rev. Lett. **94**, 107008 (2005).

[15] G. Sambandamurthy, L. W. Engel, A. Johansson, and D. Shahar, Superconductivity-Related Insulating Behavior, Phys. Rev. Lett. **92**, 107005 (2004).

[16] M. D. Stewart, A. Yin, J. M. Xu, and J. M. Valles, Superconducting Pair Correlations in an Amorphous Insulating Nanohoneycomb Film, Science **318**, 1273 (2007).

[17] P. K. Rout, I. Agireen, E. Maniv, M. Goldstein, and Y. Dagan, Six-fold crystalline anisotropic magnetoresistance in the (111) LaAlO$_3$/SrTiO$_3$ oxide interface, Phys. Rev. B **95**, 241107(R) (2017).

[18] M. Diez, A. M. R. V. L. Monteiro, G. Mattoni, E. Cobanera, T. Hyart, E. Mulazimoglu, N. Bovenzi, C. W. J. Beenakker, and A. D. Caviglia, Giant Negative Magnetoresistance Driven by Spin-Orbit Coupling at the LaAlO$_3$/SrTiO$_3$ Interface, Phys. Rev. Lett. **115**, 016803 (2015).

[19] A. Joshua, S. Pecker, J. Ruhman, E. Altman, and S. Ilani, A universal critical density underlying the physics of electrons at the LaAlO$_3$/SrTiO$_3$ interface, Nat. Commun. **3**, 1129 (2012).

[20] P. Fulde and K. Maki, Fluctuations in high field superconductors, Z. Phys. **238**, 233 (1970).

[21] K. Aoi, R. Meservey, and P. M. Tedrow, Fluctuations and the reactive transition in paramagnetically limited superconductors, Phys. Rev. B **9**, 875 (1974).

[22] L. G. Aslamazov and A. I. Larkin, The influence of fluctuation pairing of electrons on the conductivity of normal metal, Phys. Lett. A **26**, 238 (1968).

[23] S. Ullah and A. T. Dorsey, Critical Fluctuations in High-Temperature Superconductors and the Ettingshausen Effect, Phys. Rev. Lett. **65**, 2066 (1990).

[24] U. Khanna, P. K. Rout, M. Mograbi, G. Tuvia, I. Leermakers, U. Zeitler, Y. Dagan, and M. Goldstein, Symmetry and Correlation Effects on Band Structure Explain the Anomalous Transport Properties of (111) LaAlO$_3$/SrTiO$_3$, Phys. Rev. Lett. **123**, 036805 (2019).

[25] A. A. Abrikosov and L. P. Gorkov, Spin-Orbit Interaction and the Knight Shift In Superconductors, J. Exptl. Theoret. Phys. (U.S.S.R.) **42**, 1088 (1962) [Sov. Phys. JETP **15**, 752 (1962)].

[26] R. A. Klemm, A. Luther, and M. R. Beasley, Theory of the upper critical field in layered superconductors, Phys. Rev. B **12**, 877 (1975).

[27] K. Maki, Effect of Pauli Paramagnetism on Magnetic Properties of High-Field Superconductors, Phys. Rev. **148**, 362 (1966).

[28] N. R. Werthamer, E. Helfand, and P. C. Hohenberg, Temperature and Purity Dependence of the Superconducting Critical Field H$_{c2}$. III. Electron Spin and Spin-Orbit Effects, Phys. Rev. **147**, 295 (1966).

[29] J. Ruhman, A. Joshua, S. Ilani, and E. Altman, Competition between Kondo screening and magnetism at the LaAlO$_3$/SrTiO$_3$ interface, Phys. Rev. B **90**, 125123 (2014).

[30] N. Bovenzi and M. Diez, Semiclassical theory of anisotropic transport at LaAlO$_3$/SrTiO$_3$ interfaces under an in-plane magnetic field, Phys. Rev. B **95**, 205430 (2017).

[31] A. D. Caviglia, M. Gabay, S. Gariglio, N. Reyren, C. Cancellieri, and J.-M. Triscone, Tunable Rashba Spin-Orbit Interaction at Oxide Interfaces, Phys. Rev. Lett. **104**, 126803 (2010).

[32] T. Maniv and V. Zhuravlev, arXiv:2006.05098[v3].

[33] S. Ullah and A. T. Dorsey, Effect of fluctuations on the transport properties of type-II superconductors in a magnetic field, Phys. Rev. B **44**, 262 (1991).

[34] A. Bezryadin, C. N. Lau, and M. Tinkham, Quantum suppression of superconductivity in ultrathin nanowires, Nature **404**, 972 (2000).

[35] J. E. Mooij and Yu. V. Nazarov, Superconducting nanowires as quantum phase-slip junctions, Nat. Phys. **2**, 169 (2006).

[36] K. Yu. Arutyunov, D. S. Golubev, and A. D. Zaikin, Superconductivity in one dimension, Phys. Rep. **464**, 1 (2008).

[37] J. S. Lehtinen, T. Sajavaara, K. Yu. Arutyunov, M. Yu. Presnjakov, and A. L. Vasiliev, Evidence of quantum phase slip effect in titanium nanowires, Phys. Rev. B **85**, 094508 (2012); J. S. Lehtinen and K. Yu. Arutyunov, The quantum phase slip phenomenon in superconducting nanowires with a low-ohmic environment, Supercond. Sci. Technol. **25**, 124007 (2012).

[38] B. G. Orr, H. M. Jaeger, A. M. Goldman, and C. G. Kuper, Global Phase Coherence in Two-Dimensional Granular Superconductors, Phys. Rev. Lett. **56**, 378 (1986).

[39] M. P. A. Fisher, Quantum Phase Slips and Superconductivity in Granular Films, Phys. Rev. Lett. **57**, 885 (1986).

[40] S. Hurand, A. Jouan, E. Lesne, G. Singh, C. Feuillet-Palma, M. Bibes, A. Barthélémy, J. Lesueur, and N. Bergeal, Josephson-like dynamics of the superconducting LaAlO$_3$/SrTiO$_3$ interface, Phys. Rev. B **99**, 104515 (2019).

[41] John A. Hertz, Quantum critical phenomena, Phys. Rev. B **14**, 1165 (1976).

[42] H. Schmidt, The onset of superconductivity in the time dependent Ginzburg-Landau theory, Z. Phys. **216**, 336-345 (1968).

[43] A. Larkin and A. Varlamov, *Theory of fluctuations in superconductors*, The international series of monographs on physics (Clarendon Press, Oxford, 2005).

[44] T. Maniv and S. Alexander, Superconducting fluctuation effects on the local electronic spin susceptibility, J. Phys. C: Solid State Phys. **9**, 1699 (1976).

[45] J. Biscaras, N. Bergeal, S. Hurand, C. Grossetete, A. Rastogi, R. C. Budhani, D. LeBoeuf, C. Proust, and J. Lesueu, Two-Dimensional Superconducting Phase in LaAlO$_3$/SrTiO$_3$ Heterostructures Induced by High-Mobility Carrier Doping, Phys. Rev. Lett. **108**, 247004 (2012).

[46] G. Singh, A. Jouan, L. Benfatto, F. Couëdo, P. Kumar, A. Dogra, R. C. Budhani, S. Caprara, M. Grilli, E. Lesne, A. Barthélé my, M. Bibes, C. Feuillet-Palma, J. Lesueur, and N. Bergeal, Competition between electron pairing and phase coherence in superconducting interfaces, Nat. Commun. **9**, 407 (2018).

[47] M. Yang, K. Han, O. Torresin, M. Pierre, S. Zeng, Z. Huang, T. V. Venkatesan, M. Goiran, J. M. D. Coey, Ariando, and Walter Escoffier, High field magneto-transport in two-dimensional electron gas LaAlO$_3$/SrTiO$_3$, Appl. Phys. Lett. **109**, 122106 (2016).

[48] A. Kapitulnik, S. A. Kivelson, and B. Spivak, Colloquium: Anomalous metals: Failed superconductors, Rev. Mod. Phys. **91**, 011002 (2019).

[49] Y. Dubi, Y. Meir, and Y. Avishai, Nature of the superconductor–insulator transition in disordered superconductors, Nature (London) **449**, 876 (2007).

[50] K. Bouadim, Y. L. Loh, M. Randeria, and N. Trivedi, Single- and two-particle energy gaps across the disorder-driven superconductor–insulator transition, Nat. Phys. **7**, 884 (2011).

[51] A. Ghosal, M. Randeria, and N. Trivedi, Role of Spatial Amplitude Fluctuations in Highly Disordered s-Wave Superconductors, Phys. Rev. Lett. **81**, 3940 (1998).

[52] V. Vinokur, T. I. Baturina, M. V. Fistul, A. Yu. Mironov, M. R. Baklanov, and C. Strunk, Superinsulator and quantum synchronization, Nature (London) **452**, 613 (2008).